



## OPEN The two-stage prediction method for traffic spillover dissipation at short-distance intersections based on Bi-LSTM

Zijun Liang<sup>1,2,3✉</sup>, Ruihan Wang<sup>1</sup>, Xuejuan Zhan<sup>4</sup>, Tingting Hu<sup>1</sup>, Xiaoyan Li<sup>1</sup> & Yuqi Li<sup>1</sup>

In response to the common issue of traffic spillover at short-distance intersections, which tends to be overlooked due to its potential for self-dissipation, this paper conducts a study on predicting traffic spillover dissipation at short-distance intersections using the machine learning models. First, conditions for identifying traffic spillover and determining its dissipation at short-distance intersections are proposed based on traffic wave theory, and the traffic operation and data collection scenario for a short-distance intersection is built using traffic simulation software, VISSIM 11. Next, data sets required as inputs for the prediction model are collected and generated, based on queue length of stranded vehicles and the dissipation state of traffic spillover, to improve model interpretability. Finally, a two-stage prediction model for traffic spillover dissipation is constructed using a Bi-LSTM model. The first stage of the model predicts the queue length of stranded vehicles on the road segment, which is then used as feature data for the second stage to predict the spillover dissipation state between short-distance intersections. The results show that the model's prediction of the queue length of stranded vehicles in the first stage outperforms the DT, CNN, RF, LSTM, and GRU models, with a prediction accuracy of 93.4%, which verifies the feasibility of selecting the Bi-LSTM model in this paper. The model's prediction of traffic spillover dissipation state in the second stage outperforms single-stage prediction models, with the model achieving an accuracy of 92.88% in traffic spillover identification and 90.72% in traffic spillover dissipation state prediction. This validates the effectiveness of the two-stage prediction method proposed in this paper and is conducive to further improving the model's prediction accuracy. The proposed method can accurately predict traffic spillover and their dissipation at short-distance intersections, enabling the targeted selection of signal control strategies to address traffic spillover issues, thereby effectively improving the capacity of short-distance intersections.

**Keywords** Traffic spillover, Bi-LSTM, Queue length of stranded vehicles, Traffic spillover dissipation state, Two-stage prediction method

With rapid urbanization, urban roads are continuously expanding, and intersections within the road network are becoming increasingly dense, resulting in many intersections with short connecting segments, known as short-distance intersections<sup>1</sup>. Due to the limited space for queuing vehicles in these short segments and the influence of traffic signals from both upstream and downstream intersections, traffic spillover often occurs—where the queue length of vehicles at a downstream intersection exceeds the segment length and spills over into the upstream intersection<sup>2</sup>. Severe traffic spillover can lead to gridlock across the entire road network, making the identification and control of traffic spillover a focal point in current traffic management research.

Over the past decade, numerous methods have been developed for identifying traffic spillover state. The most fundamental approach involves installing detectors such as loops, radars, and video cameras at the exits of upstream intersections<sup>3,4</sup>, and determining whether queue length spillover occurs at downstream intersections by monitoring vehicle occupancy rates<sup>5</sup>. Although these methods can identify traffic spillover, their effectiveness is limited by the detection range of the detectors. Therefore, some studies<sup>6–9</sup> have established spillover indices

<sup>1</sup>School of Urban Construction and Transportation, Hefei University, Hefei 230601, China. <sup>2</sup>Anhui Province Transportation Big Data Analysis and Application Engineering Laboratory, Hefei 230601, China. <sup>3</sup>Anhui Provincial Key Laboratory of Urban Rail Transit Safety and Emergency Management, Hefei 230601, China. <sup>4</sup>School of Environment and Energy Engineering, Anhui Jianzhu University, Hefei 230601, China. ✉email: lzj@hfuu.edu.cn

or algorithmic models based on collected traffic data such as flow, queue length, speed, and density to identify traffic spillover state in real time, providing insights for the traffic spillover identification research in this paper. Additionally, these traffic spillover identification methods lay the foundation for traffic spillover control. Most current studies immediately implement traffic spillover control measures after identifying spillover to reduce vehicle queue length and address intersection spillover issues<sup>9</sup>. While these measures improve queue spillover to some extent, they also restrict the normal flow of merging vehicles, increasing intersection delays, and overlook the possibility of traffic spillover dissipating on their own. This is particularly relevant in short-distance segments between intersections, typically ranging from 50 to 200 m, where traffic spillover occurs frequently<sup>10</sup>. If traffic signal is adjusted immediately each time spillover occurs, the frequent changes in signal plans may hinder vehicle flow at short-distance intersections, significantly impacting their traffic capacity. Therefore, for short-distance intersections, if traffic spillover can be identified in advance through predictive methods, and further predictions are made to determine whether the spillover will dissipate in time, signal control strategies can be selectively applied to address the issue. Consequently, we focus on short-distance intersections and propose to conduct research on predicting the dissipation of traffic focus based on its identification.

Additionally, the above studies reveal that vehicle queue length is crucial for identifying and dissipating traffic spillover. Currently, many researchers have conducted studies on queue length estimation and prediction. Some studies directly estimate and predict queue length<sup>11–13</sup>. However, due to the high dynamics and uncertainty of traffic systems, factors such as traffic flow, vehicle speed, and signal timing are constantly changing, resulting in queue length lacking obvious patterns<sup>14</sup>. This makes it difficult to directly and accurately predict future queue length. To address this, indirect estimation and prediction methods have emerged<sup>15–18</sup>, which indirectly predict queue length by analyzing or forecasting parameters such as traffic flow<sup>15</sup>, cycle time<sup>16,17</sup>, and offset<sup>18</sup>. These methods offer advantages such as easy data acquisition, controllable accuracy, obvious periodic variation characteristics, and good queue length prediction performance. Therefore, machine learning models can be further employed to predict queue length by integrating the above-mentioned data.

At present, machine learning models commonly used for traffic data prediction include Decision Tree (DT), Convolutional Neural Network (CNN), Random Forest (RF), Long Short-Term Memory Network (LSTM), and Gated Recurrent Unit (GRU). Compared with DT, CNN and RF models, LSTM and GRU are more suitable for processing and predicting important events with relatively long intervals and delays in time series, demonstrating higher prediction accuracy in some traffic application scenarios<sup>19,20</sup>. However, since LSTM and GRU can only process sequential data in a forward direction and cannot capture reverse contextual information, while the current state of traffic data is related to both past and future states, models that can handle long-term dependencies in time series and capture contextual information in both forward and backward directions are preferred. For example, the Bidirectional Long Short-Term Memory Network (Bi-LSTM) model, through the mechanisms of forget gate, input gate, and output gate, can more finely control the flow and storage of information in time series, making it more accurate and effective in capturing and utilizing long-term dependent information. Additionally, its feature of capturing contextual information in both directions allows the model to consider both past and future contexts simultaneously<sup>21</sup>, making it potentially more suitable for traffic data prediction. Therefore, this paper proposes using the Bi-LSTM model for prediction.

Based on the above analysis, the formation and dissipation of traffic spillover are closely related to vehicle queue length, which in turn is influenced by intersection flow, cycle time, and offset schemes. Therefore, the main approach of this study on traffic spillover identification and dissipation prediction for short-distance intersections is as follows: First, using intersection flow, cycle time, offset, and other relevant traffic data, the Bi-LSTM model is applied to predict the queue length of stranded vehicles. On this basis, further research is conducted on traffic spillover identification and dissipation prediction by integrating the predicted queue length of stranded vehicles with other relevant traffic data. Therefore, we address the problem of traffic spillover identification and dissipation prediction for short-distance intersections through the following three innovative contributions. First, by combining traffic wave theory, it proposes criteria for identifying and distinguishing traffic spillover and dissipation at short-distance intersections, laying the foundation for predicting traffic spillover dissipation at such intersections. Second, it constructs the input data set required for the machine learning prediction model by utilizing methods for calculating the queue length of stranded vehicles on the segment and the traffic spillover dissipation state, thereby improving the model's interpretability. Third, based on the Bi-LSTM model, it develops a two-stage prediction model, where the queue length of stranded vehicles predicted in the first stage serves as feature data for the second stage, effectively enhancing the prediction accuracy of traffic spillover dissipation.

The remainder of this paper is organized as follows. The literature review is introduced in Sect. "[Literature review](#)". The research methodology is introduced in Sect. "[Method](#)". The case study results are presented in Sect. "[Results](#)". The findings and the reasons behind these results are discussed in Sect. "[Discussion](#)". The conclusions are given in Sect. "[Conclusions](#)".

## Literature review

In terms of traffic spillover state identification, Geroliminis et al.<sup>22</sup> proposed a method to identify spillover through changes in occupancy rate detected by loop detectors, and provided an occupancy threshold for spillover occurrence. Shi Xiaowei et al.<sup>3</sup> used video detectors to obtain real-time queue length on road segments to identify traffic spillover state. Ren et al.<sup>4</sup> proposed a method to identify vehicle queue spillover based on actual speed measurements from detectors. Wu et al.<sup>23</sup> used high-resolution traffic signal data to measure spillover index at oversaturated intersections in either the temporal or spatial dimension. Zhang Lidong et al.<sup>6</sup> proposed a fuzzy recognition algorithm for traffic spillover based on vehicle queue ratio and average segment speed as input data, grounded in the theory of intelligent fuzzy inference. Ma et al.<sup>7</sup> proposed a method to determine the spillover threshold occupancy using traffic flow data collected from upstream fixed detectors. Zhu Renwei et al.<sup>8</sup> based on detector data and traffic wave theory, proposed a vehicle spillover identification model for bottleneck

sections by comparing the maximum generalized queue length with the spillover safety distance. Zhang et al.<sup>9</sup> using advanced wide-area radar detection data, established a comprehensive spillover identification index with average speed and space occupancy as sub-indicators. Zhang et al.<sup>24</sup> used the unmanned aerial vehicle remote sensing for preliminary identification of intersection spillover. The above studies show that most research can identify traffic spillover state in real time through detectors or by establishing spillover indicators and algorithm models, but there is relatively little research on predicting traffic spillover state.

In terms of traffic spillover control, Zhang et al.<sup>9</sup> immediately applied a matched control strategy based on the traffic demand in the non-spillover phase of the signalized intersection after detecting traffic spillover through wide-area radar, in order to control the queue length of the traffic spillover. Cesme et al.<sup>25</sup> proposed a self-organizing control logic for oversaturated intersection, where, if the spillover detector identifies spillover on the main road, it immediately reduces the green light time for the side road and extends that for the main road to reduce spillover queue length. Zhang Lidong et al.<sup>26</sup> optimized the signal control plan through an intelligent traffic spillover coordination control algorithm immediately after detecting traffic spillover, allowing the queue of spillover vehicles to gradually dissipate. Yao et al.<sup>27</sup> upon detecting traffic spillover, immediately used fuzzy control to reallocate green light time for the spillover direction. By implementing minimal, shortened, or no green light, they restricted merging vehicles and promptly controlled the spillover queue length. The above methods immediately control traffic after spillover occurs at intersections by adjusting traffic signal to restrict vehicle merging or facilitate vehicle dispersal. This reduces queue length, allowing spillover vehicles to dissipate, indicating that queue length has a significant impact on the dissipation of traffic spillover. The above studies indicate that most research adopts traffic spillover control measures immediately after identifying spillover to reduce vehicle queue lengths and address intersection spillover issues. However, these measures restrict the normal flow of merging vehicles, leading to increased intersection delays, and overlook the possibility of traffic spillovers dissipating spontaneously.

In terms of queue length estimation and prediction, Lee et al.<sup>11</sup> developed a real-time lane-based queue length prediction method using CNN and LSTM algorithms. Rahman R et al.<sup>12</sup> used a LSTM to predict queue length for the next cycle. Comert et al.<sup>13</sup> applied traffic wave theory and the Robertson dispersion model to predict traffic queue length in real-time. However, due to the high dynamics and uncertainty of traffic systems, it is difficult to directly and accurately predict future queue length. Therefore, some indirect estimation and prediction methods have emerged. Dai et al.<sup>15</sup> suggested that queue length increases continuously with a sharp rise in traffic flow and developed a queue length prediction model based on deterministic queuing theory, building on traffic flow forecasting. Liu et al.<sup>16</sup> based on traffic wave theory and high-resolution traffic signal data, proposed a method to predict the current cycle's queue length by performing regression analysis on the previous cycle's queue length. Yao et al.<sup>18</sup> considering the offset between upstream and downstream intersections, proposed a periodic vehicle queue length estimation method based on fixed detector data. Zhao et al.<sup>28</sup> proposed a probabilistic approach to establish and solve a single-variable formula for detecting vehicle penetration rates, which can be used to estimate penetration rates and predict traffic flow and queue length. Abewickrema et al.<sup>17</sup> proposed a novel multivariate time-varying Kalman filter approach to estimate the cycle-based maximum queue lengths in real-time by only using high-resolution vehicle loop detector data and signal timing data. The above studies indicate that queue length can be predicted through direct or indirect methods, but indirect queue length prediction methods are superior, offering advantages such as easy data acquisition, controllable accuracy, obvious periodic variation characteristics, and good queue length prediction performance.

In terms of traffic data prediction based on machine learning models, Xia et al.<sup>29</sup> proposed a traffic flow forecasting method based on gradient boosting DT. Fu et al.<sup>30</sup> proposed a traffic data prediction method that integrates Transformer and CNN based on various nonlinear spatial relationships of correlated intersections and the potential temporal dependencies in traffic volume. Wumaier et al.<sup>31</sup> introduced a dynamic traffic data prediction method based on the RF algorithm. Katambire et al.<sup>19</sup> used LSTM and the Auto Regressive Integrated Moving Average model to predict future traffic rates. The results showed that LSTM is the best-fitting model for monthly traffic data prediction. However, compared with DT, CNN, RF, LSTM and GRU models, the Bi-LSTM model can process both forward and backward sequence information, which can not only utilize the traffic state information at past moments, but also consider the impact of future moments on the current state, and capture more comprehensive time-series features. Therefore, some scholars have carried out research on traffic data prediction based on the Bi-LSTM model. For example, Ma et al.<sup>32</sup> proposed a short-term traffic flow prediction model based on time series analysis of traffic flow and Bi-LSTM to improve prediction accuracy and deeply explore the spatiotemporal characteristics of traffic flow data. Ounoughi C et al.<sup>33</sup> introduced a Bi-LSTM-based model for traffic speed prediction. Abduljabbar R L et al.<sup>21</sup> used simulation data to develop a Bi-LSTM short-term traffic prediction model, and the results showed that Bi-LSTM performed exceptionally well across multiple prediction horizons for all traffic variables. The above studies indicate that traffic data can be predicted through various machine learning models, but Bi-LSTM with the feature of capturing contextual information in both forward and backward directions has better prediction performance.

In summary, most research on traffic spillover focuses on real-time identification through detectors or spillover indices, with limited studies on traffic spillover prediction. Additionally, most traffic spillover control measures are implemented after spillover occurs, overlooking the possibility of spontaneous dissipation. Meanwhile, queue length is crucial for identifying and dissipating traffic spillover, and future queue lengths can be better predicted indirectly. On this basis, the Bi-LSTM model can be used to predict traffic spillover and its dissipation at short-distance intersections, providing a predictive method for the advanced management and control of traffic spillover at such intersections.

### Method

#### Traffic spillover identification and dissipation criteria

Consider a short-distance intersection as shown in Fig. 1, where the upstream and the downstream intersection is denoted as  $O_1$  and  $O_2$ , the internal distance is  $l_n$ . The segment between  $O_1$  and  $O_2$  in the westbound direction is the segment where traffic spillover dissipation analysis is conducted (hereafter referred to as the “segment”), with a length of  $L_n$ . The signal cycle time at both  $O_1$  and  $O_2$  is  $C$ , with green light duration for westbound traffic being  $g_1$  and  $g_2$ , respectively. The offset (i.e., the difference between the green light start times at  $O_1$  and  $O_2$ , with the green light start time at  $O_2$  as the reference) is  $t_f$ .

The queue length of stranded vehicles on the segment during the previous signal cycle at  $O_2$  is  $L$ . When the green light at  $O_1$  starts during the current cycle, vehicles depart at a speed of  $u_1$  toward the segment. When they encounter queuing vehicles on the segment, they stop and form a stopping wave with a wave speed of  $u_{tw}$ . During the current signal cycle at  $O_2$ , the queuing vehicles on the segment begin to leave at a speed of  $u_2$ , forming a starting wave with a wave speed of  $u_{qw}$ . When the stopping wave and the starting wave meet at point A, the vehicle queue length on the segment reaches its maximum,  $L_{max}$ . According to traffic wave theory<sup>34</sup>, formulas (1) to (3) hold at this point.

$$u_{tw}(t_{qs} + t_f - t_1) = u_{qw}(t_{qs} - \frac{L}{u_{qw}}) \tag{1}$$

$$t_{qs} = \frac{L + (t_f - t_1)u_{tw}}{u_{qw} - u_{tw}} \tag{2}$$

$$t_1 = \frac{L_n - L + l_n}{u_1} \tag{3}$$

where  $t_{qs}$  is the dissipation time of queuing vehicles on the road segment, and  $t_1$  is the time taken for the first vehicle entering from  $O_1$  after the green light at  $O_1$  to reach the end of the queuing vehicles on the road segment in Fig. 1. The maximum vehicle queue length  $L_{max}$  for a road section can be calculated using formula (4)

$$L_{max} = t_{qs} \cdot u_{qw} = \frac{L + (t_f - t_1)u_{tw}}{u_{qw} - u_{tw}} \cdot u_{qw} \tag{4}$$

By substituting formula (3) into formula (4), the difference between  $L_{max}$  and  $L_n$  is obtained  $\Delta L$ , resulting in formula (5).

$$\Delta L = L_{max} - L_n = \frac{L \cdot u_1 + (L - l_n + t_f u_1)u_{tw}u_{qw} - L_n(u_{tw}u_{qw} + u_1(u_{qw} - u_{tw}))}{u_1(u_{qw} - u_{tw})} \tag{5}$$

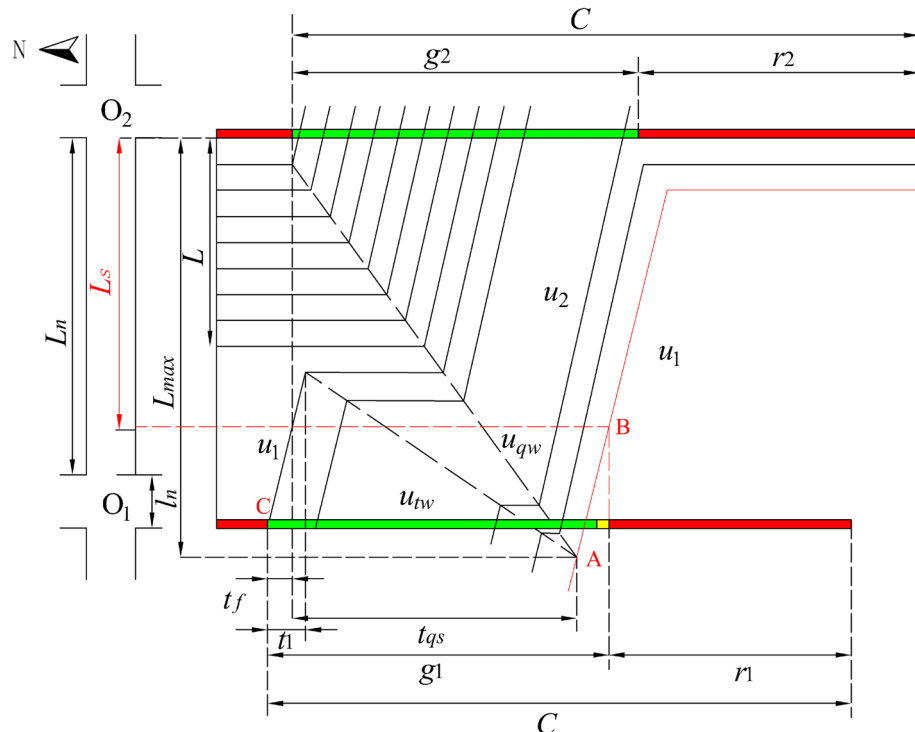
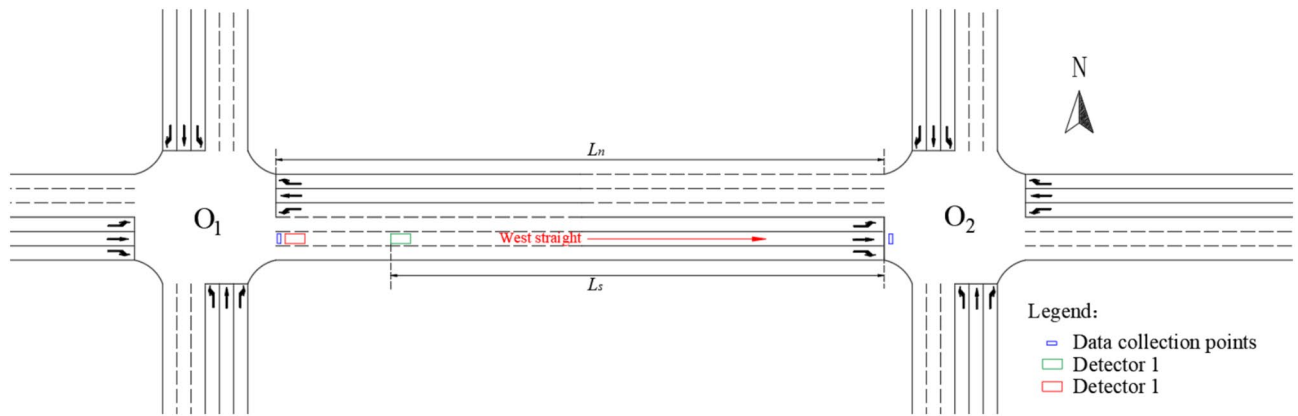


Fig. 1. Analysis of traffic spillover dissipation between short-distance intersections.



**Fig. 2.** Layout of detectors and data collection points.

| $S_{g1i}$ | $S_{g2i}$ | $S_{r1i}$ | $S_{r2i}$ | $P_i$ | State determination and optimization strategy  |
|-----------|-----------|-----------|-----------|-------|--|
| 0 or 1    | 0         | 0         | 0         | 1     | No traffic spillover occurs; spillover control is not required   |
| 1         | 1         | 0         | 0         | 2     | Effectively dissipating traffic spillover occurs; spillover control is not required  |
| 1         | 1         | 1         | 0         | 3     | Potentially non-dissipating traffic spillover occurs; spillover control is required, and the signal timing plan should be adjusted accordingly |
| 1         | 1         | 1         | 1         | 4     | Absolutely non-dissipating traffic spillover occurs; spillover control is required, and the signal timing plan should be readjusted            |

**Table 1.** Determination and optimization strategy for traffic spillover dissipation state.

From formula (5), it can be understood that when  $\Delta L < 0$ , traffic spillover will not occur in the current cycle; conversely, when  $\Delta L \geq 0$ , it indicates that traffic spillover will occur (as shown in Fig. 1) and is closely related to the maximum queue length. Given that  $u_{qw} > u_{tw}$ , if  $L$  increases and  $L_n$  decreases,  $\Delta L$  is more likely to exceed 0, thus increasing the likelihood of traffic spillover. When traffic spillover occurs, it can be determined whether the spillover will dissipate by checking if the last vehicle spilling before the red light at  $O_1$  can reach the safe distance  $L_s$  within the road section. This distance ensures that vehicles merging from other directions (taking a left turn north and a right turn south) during the red light time  $r_1$  for  $O_1$  in Fig. 1 will not spillover into  $O_1$ . The relationship is expressed as follows.

$$L_s + (Q_{Nl} \cdot w_1 + Q_{Sr} \cdot w_2) H_d \leq L_n \tag{6}$$

where  $Q_{Nl}$  and  $Q_{Sr}$  are the number of vehicles taking a left turn north and a right turn south toward  $O_2$  during the  $r_1$  at  $O_1$  in Fig. 1, respectively.  $w_1$  and  $w_2$  represent the proportion of vehicles in  $Q_{Nl}$  and  $Q_{Sr}$  that enter the road section, and  $H_d$  is the average headway between vehicles.

When the last vehicle involved in the traffic spillover before the red light at  $O_1$  in Fig. 1 reaches point B within the safe distance  $L_s$ , and no spillover occurs during the red light time  $r_1$  at  $O_1$ , it indicates that the spillover can dissipate in time within the green light at  $O_2$ . In this case, spillover control is not required; otherwise, spillover control is needed. To detect both traffic spillover and its dissipation, detectors 1 and 2 are placed at the safe distance and at the end of the road, respectively, as shown in Fig. 2. The vehicle occupancy states for the green and red lights at the  $i$ -th cycle at upstream intersection  $O_1$  in Fig. 1 are recorded as  $S_{g1i}$ ,  $S_{g2i}$ ,  $S_{r1i}$  and  $S_{r2i}$  respectively. These states are used to determine the spillover dissipation state  $P_i$  of the short-distance intersections during the  $i$ -th cycle.

The values of  $S_{g1i}$ ,  $S_{g2i}$ ,  $S_{r1i}$  and  $S_{r2i}$  are either 0 or 1. A value of 1 is assigned when a vehicle's occupancy time at the detector reaches a certain threshold (e.g., 10 s), indicating that vehicles are queued up to the location of the detector; otherwise, the value is 0. Based on this, the determination and optimization strategy for the traffic spillover dissipation state  $P_i$  is shown in Table 1.

In Table 1, the values of  $P_i$  are categorized into four scenarios: When  $P_i = 1$ , no traffic spillover occurs, so spillover control is not required. When  $P_i = 2$ , effectively dissipating traffic spillover occurs. This means that spillover happens only during the green light at  $O_1$  in Fig. 1 and dissipates before the green light ends. The queue length of vehicles remaining on the road is within the safe distance before the red light at  $O_1$  begins, so spillover control is not required.

When  $P_i = 3$ , it indicates the occurrence of potential non-dissipating traffic spillover, which means that traffic spillover happens during the green light period of  $O_1$  in Fig. 1. Before the red light starts, the queue length of stagnant vehicles from the spillover reaches or exceeds the safe distance. Although this queue length has not yet exceeded the road segment length  $L_n$ , there remains a potential spillover risk. Therefore, spillover control measures need to be implemented, and the signal timing plan can be appropriately adjusted. When  $P_i = 4$ , absolutely non-dissipating traffic spillover occurs. This means that spillover occurs during both the green and

red times at  $O_1$  in Fig. 1 and cannot dissipate in time, requiring spillover control and a readjustment of the signal timing plan.

Through the setting of the above traffic spillover identification and dissipation discrimination conditions, it is convenient to determine whether spillover occurs between short-distance intersections and whether the spillover can dissipate, providing a basis for traffic spillover dissipation prediction.

### Data collection approach and methods

Currently, commonly used spillover control methods mainly address the traffic spillover issue by adjusting three conditions: input flow rate<sup>15</sup> signal cycle<sup>16</sup>, and offset<sup>18</sup>. These factors significantly impact the dissipation of traffic spillover, and when they change, traffic parameters such as the number of vehicles arriving and leaving at the road, average speed, and average density will also vary. Therefore, in this study, a simulation road network with the short-distance intersections was built in VISSIM 11. Different data collection schemes corresponding to varying input flow rates  $Q$ , cycle time  $C$ , and offset  $t_f$  were set to obtain the required data.

As shown in Fig. 3,  $Q$  is set with 10 schemes, each simulating the peak variation of traffic flow during peak hours. For each scheme, 12 different flow values  $Q_i$  are selected, with one value chosen every 6 cycles in sequence.  $C$  is set with 9 values: 80s, 90s, 100s, 110s, 120s, 130s, 140s, 150s, and 160s.  $t_f$  is set with 9 values: -20s, -15s, -10s, -5s, 0s, 5s, 10s, 15s, and 20s. Using the above method, a total of 810 ( $10 \times 9 \times 9$ ) data collection schemes can be formed, as shown in Fig. 3. Since the flow values  $Q_i$  change every 6 cycles, each data collection scheme will generate data for 72 ( $12 \times 6$ ) cycles. In total, 58,320 ( $810 \times 72$ ) cycles of data can be collected.

To collect the required data, data collection points are first set at the end of the road segment and in front of the stop line (as shown in Fig. 2), which are used to collect the number of vehicles arriving at the road segment  $Q_{1i}$ , the number of vehicles departing  $Q_{2i}$ , the average speed  $v_i$ , and the average density  $k_i$  for each cycle. Based on the number of vehicles arriving and leaving collected each cycle, the number of vehicles stranded on the road  $R_i$  and the queue length of the stranded vehicles  $L_i$  can be calculated. The calculation formulas are as follows:

$$R_i = Q_{1i} - Q_{2i}, i = 1 \tag{7}$$

$$R_i = R_{i-1} + Q_{1i} - Q_{2i}, i \geq 2 \tag{8}$$

$$L_i = \frac{R_i}{n_L} \cdot H_d \tag{9}$$

where  $R_i$  and  $R_{i-1}$  are the number of vehicles stranded on the road in the  $i$ -th and  $i-1$ -th cycles, respectively;  $Q_{1i}$  and  $Q_{2i}$  are the number of vehicles arriving at and leaving the road in the  $i$ -th cycle, respectively;  $L_i$  is the queue length of the stranded vehicles on the road in the  $i$ -th cycle;  $H_d$  is the average headway between vehicles, typically taken as 7 m; and  $n_L$  is the number of lanes on the road.

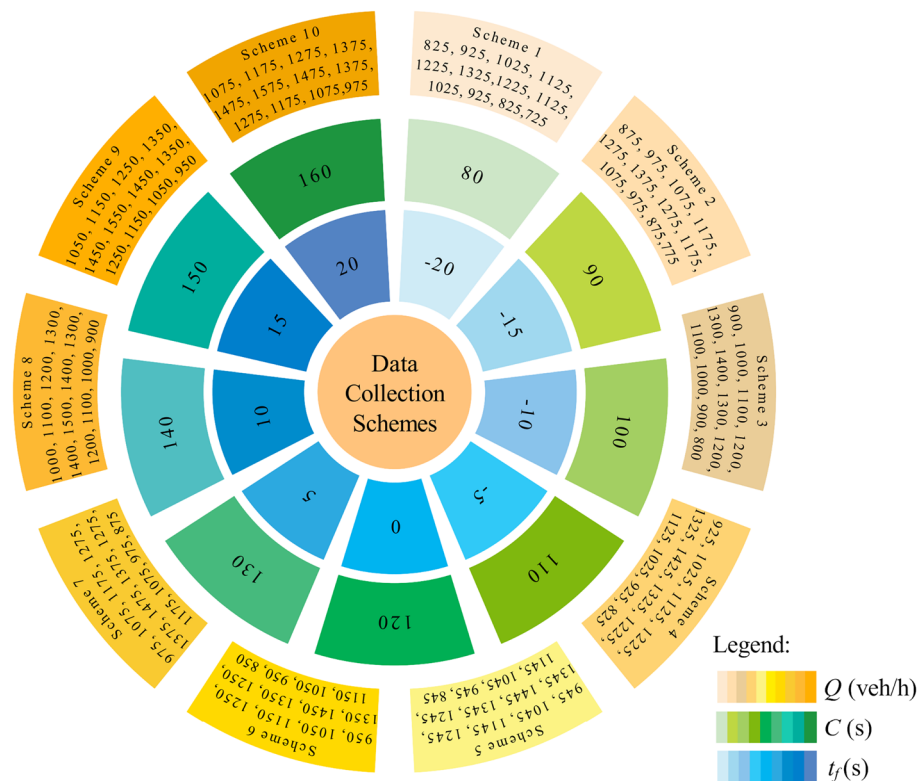


Fig. 3. Data collection scheme setup.

Based on formulas (7) and (8), it can be seen that if the number of vehicles stranded on the road in the first cycle,  $R_1$ , is unknown, it is not possible to calculate the stranded vehicles for subsequent cycles, meaning the queue length of stranded vehicles for any future cycle cannot be directly computed. Therefore, it is necessary to collect  $Q_{1i}$  and  $Q_{2i}$  for each cycle and calculate  $R_i$  and  $L_i$  according to formulas (7) to (9). The data set including  $Q_{1i}$ ,  $Q_{2i}$ ,  $R_i$ ,  $L_i$ ,  $v_i$ , and  $k_i$  will be incorporated into the machine learning model as input data, which can be used to predict the queue length of stranded vehicles for a future cycle.

The occupancy states  $S_{g1i}$ ,  $S_{g2i}$ ,  $S_{r1i}$  and  $S_{r2i}$  for each cycle must be collected through detector 1 and detector 2 in Fig. 2. Specifically, this can be achieved by developing a COM interface program for VISSIM 11, which will allow the calculation of the traffic spillover dissipation state  $P_i$  for each cycle using Table 1. These data will also be included in the input data set for the machine learning model, allowing it to further predict the traffic spillover dissipation state for a future cycle. Therefore, the final data to be collected in different data collection schemes, as shown in Table 2, will effectively enhance the interpretability of the prediction model.

Through the setting of the above data collection ideas and methods, the data required in this paper and the reasons for collecting these data are intuitively displayed, which effectively improves the interpretability of the Bi-LSTM model and provides a data foundation for the subsequent construction of the prediction model.

### Sensitivity analysis

Since  $Q$ ,  $C$  and  $t_f$  all have significant impacts on the traffic spillover dissipation state  $P$  of the road segment, this paper uses the local sensitivity analysis method<sup>36</sup> to explore whether there is a causal relationship between the above factors and the traffic spillover dissipation state of the road segment, providing a basis for selecting input data for the traffic spillover dissipation prediction model. Drawing on the theory of this method, this paper takes  $Q$ ,  $C$ , and  $t_f$  as features and  $P$  as the target variable to analyze the influence of each feature on the target variable. The specific methods are as follows.

Taking the three factors  $Q$ ,  $C$ , and  $t_f$  as features, and using their current values  $Q_0$ ,  $C_0$  and  $t_{f0}$  as benchmark values respectively, the variation ranges of the features are set according to the benchmark values, as shown in formulas (10) to (12).

$$Q_i \in [Q_0 - \Delta Q, Q_0 + \Delta Q] \tag{10}$$

$$C_i \in [C_0 - \Delta C, C_0 + \Delta C] \tag{11}$$

$$t_{fi} \in [t_{f0} - \Delta t_f, t_{f0} + \Delta t_f] \tag{12}$$

where  $Q_i$ ,  $C_i$ , and  $t_{fi}$  are the values of  $Q$ ,  $C$ , and  $t_f$  in the  $i$ -th cycle, and  $\Delta Q$ ,  $\Delta C$ , and  $\Delta t_f$  are the variations in  $Q$ ,  $C$ , and  $t_f$  respectively.

Under the premise that other features remain at their baseline values, a specific feature takes different values within its range of variation, and the corresponding traffic spillover dissipation state  $P_i$  is obtained. For example, when  $C$  and  $t_f$  are set to their baseline values  $C_0$  and  $t_{f0}$ , and  $Q$  takes different values  $Q_i$  within its range, the data  $S_{g1i}$ ,  $S_{g2i}$ ,  $S_{r1i}$  and  $S_{r2i}$  are output by the VISSIM 11, from which the corresponding values of  $P_i$  can be derived. This allows for an analysis of the impact of each factor on the traffic spillover dissipation state.

Therefore, referring to the traffic operation conditions of actual short-distance intersections, this paper first sets the current values of the three features—input  $Q$ ,  $C$ , and  $t_f$ —are set to 1300 veh/h, -5s, and 100s, respectively. When  $Q$  is analyzed as a single factor,  $C$  and  $t_f$  are fixed at their current values. The value of  $Q$  is set according to Scheme 3 in Fig. 3, ranging from 900 veh/h to 1400 veh/h, and then decreased to 800 veh/h, with a change of 100 veh/h every 600 s (6 cycles). The simulation runs for 7200 s. Similarly, when  $C$  is analyzed as a single factor,  $Q$  and  $t_f$  are fixed at their current values, and  $C$  is set to range from 80 to 160s, with each cycle running 30 times. When  $t_f$  is analyzed as a single factor,  $Q$  and  $C$  are fixed at their current values, and  $t_f$  is set to range from -20s to 20s, with an increment of 5s every 3600 s (36 cycles). The simulation runs for 32,400 s. Then, the required data, similar to the data in Table 3, are collected and calculated from the VISSIM 11 for each cycle, enabling the analysis of the impact of each feature on the  $P$ .

Through the above sensitivity analysis setup, it is convenient to determine whether the three features  $Q$ ,  $C$ , and  $t_f$  affect traffic spillover dissipation and the magnitude of their impacts, providing ideas for the design of data collection schemes.

### Two-stage prediction model of traffic spillover dissipation based on Bi-LSTM

#### Bi-LSTM model theory

Bi-LSTM has strong sequence modeling capabilities, allowing it to model and predict the time series features of traffic data. Bi-LSTM is composed of two LSTM units in opposite directions, and each unidirectional LSTM unit mainly includes a forget gate, a memory gate, and an output gate, which enables it to better process information with long time spans. The structure is shown in Fig. 4.

Assume the input data series is  $x_1, x_2, \dots, x_t$  and the output signals are  $h_1, h_2, \dots, h_t$ . The relevant formulas are as follows.

$$f_t = \sigma(W_f \cdot [h_{t-1}, x_t] + b_f) \tag{13}$$

|       |       |          |          |          |       |       |       |       |           |           |           |           |       |
|-------|-------|----------|----------|----------|-------|-------|-------|-------|-----------|-----------|-----------|-----------|-------|
| $Q_i$ | $C_i$ | $t_{fi}$ | $Q_{1i}$ | $Q_{2i}$ | $R_i$ | $L_i$ | $v_i$ | $k_i$ | $S_{g1i}$ | $S_{g2i}$ | $S_{r1i}$ | $S_{r2i}$ | $P_i$ |
|-------|-------|----------|----------|----------|-------|-------|-------|-------|-----------|-----------|-----------|-----------|-------|

**Table 2.** Data to be collected for different data collection schemes.

| No  | $Q_i$ | $C_i$ | $t_{fi}$ | $Q_{1i}$ | $Q_{2i}$ | $R_i$ | $L_i$ | $v_i$ | $k_i$ | $S_{g1i}$ | $S_{g2i}$ | $S_{r1i}$ | $S_{r2i}$ | $P_i$ |
|-----|-------|-------|----------|----------|----------|-------|-------|-------|-------|-----------|-----------|-----------|-----------|-------|
| 1   | 950   | 100   | -5       | 1        | 0        | 0     | 0     | 49.65 | 0.7   | 0         | 0         | 0         | 0         | 1     |
| ... | ...   | ...   | ...      | ...      | ...      | ...   | ...   | ...   | ...   | ...       | ...       | ...       | ...       | ...   |
| 20  | 1250  | 100   | -5       | 17       | 16       | 11    | 77    | 33.17 | 18.5  | 1         | 1         | 0         | 0         | 2     |
| ... | ...   | ...   | ...      | ...      | ...      | ...   | ...   | ...   | ...   | ...       | ...       | ...       | ...       | ...   |
| 31  | 1450  | 100   | -5       | 17       | 16       | 12    | 84    | 30.5  | 20.1  | 1         | 1         | 1         | 1         | 4     |
| ... | ...   | ...   | ...      | ...      | ...      | ...   | ...   | ...   | ...   | ...       | ...       | ...       | ...       | ...   |
| 43  | 1250  | 100   | -5       | 16       | 15       | 10    | 70    | 34.92 | 16.5  | 1         | 1         | 1         | 1         | 4     |
| ... | ...   | ...   | ...      | ...      | ...      | ...   | ...   | ...   | ...   | ...       | ...       | ...       | ...       | ...   |
| 72  | 850   | 100   | -5       | 9        | 10       | 3     | 21    | 51.35 | 6.3   | 0         | 0         | 0         | 0         | 1     |

**Table 3.** Partial collected data.

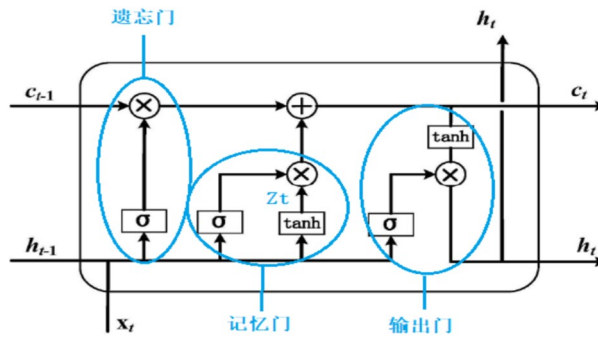


**Fig. 4.** Structure of unidirectional LSTM unit.

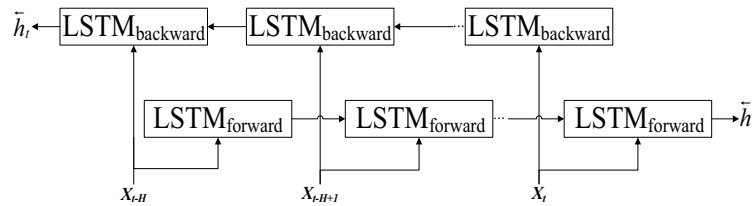


**Fig. 5.** Bi-LSTM model structure.

$$i_t = \sigma(W_i \cdot [h_{t-1}, x_t] + b_i) \tag{14}$$

$$\tilde{c}_t = \tanh(W_c \cdot [h_{t-1}, x_t] + b_c) \tag{15}$$

$$c_t = f_t c_{t-1} + i_t \tilde{c}_t \tag{16}$$

$$o_t = \sigma(W_o \cdot [h_{t-1}, x_t] + b_o) \tag{17}$$

$$h_t = o_t \tanh(c_t) \tag{18}$$

where  $f_t$  is the forget gate,  $i_t$  is the input gate,  $c_t$  is the updated cell state, and  $o_t, h_t$  are the output gate.  $W_p, b_p, W_p, b_p, W_c, b_c, W_o$  and  $b_o$  denote the neural network parameters.  $\sigma()$  is the sigmoid neural network layer, and  $\tanh()$  is the  $\tanh$  neural network layer and the  $\tanh$  activation function in Eqs. (15) and (18), respectively.

Since the Bi-LSTM model is composed of two LSTM units in opposite directions, it can process time-series data along both forward and backward time steps, fully considering information from historical and future moments. By integrating information from preceding and succeeding moments, it can better capture the dynamic changes in traffic data. The model structure is shown in Fig. 5. The structures of the Bi-LSTM model are intuitively displayed through Fig. 4 and Fig. 5, which improves the interpretability of the prediction model.

The forward implicit vector  $\overleftarrow{h}_{t-1}$  generates a new implicit vector  $\overleftarrow{h}_t$ , and the backward implicit vector  $\overrightarrow{h}_{t-1}$  generates a new implicit vector  $\overrightarrow{h}_t$ . By combining the output results of both the forward and backward input sequences, we obtain  $Y_t$ . The specific calculation is as follows.

$$\vec{h}_t = \text{LSTM} \left( x_t, \vec{h}_{t-1} \right) \tag{19}$$

$$\overleftarrow{h}_t = \text{LSTM} \left( x_t, \overleftarrow{h}_{t-1} \right) \tag{20}$$

$$Y_t = \tanh \left( w_{\vec{h}_y} \vec{h}_t + w_{\overleftarrow{h}_y} \overleftarrow{h}_t + b_y \right) \tag{21}$$

where  $\vec{h}_t$  and  $\overleftarrow{h}_t$  are the outputs of the forward and backward hidden layers at time step  $t$ , respectively;  $w_{\vec{h}_y}$  and  $w_{\overleftarrow{h}_y}$  represent the weight matrices connecting each layer to the previous hidden state; and  $b_y$  denotes the bias term.

*Data input and output of the prediction model*

The commonly used model prediction method involves directly outputting the prediction results after inputting the data (i.e., single-stage prediction). However, as shown in Sections "Traffic spillover identification and dissipation criteria" and "Data collection approach and methods" of this paper, the queue length of stranded vehicles affects the traffic spillover situation on the road, and the queue length of stranded vehicles in a future cycle cannot be directly calculated or obtained. Therefore, we propose a two-stage traffic spillover dissipation prediction model based on Bi-LSTM. In the first stage, the Bi-LSTM model is used to predict the queue length of stranded vehicles on the road. After verifying that the first stage prediction results meet the required criteria, these results are used as one of the feature inputs for the second stage prediction. Combined with other input data in the second stage to jointly predict the traffic spillover dissipation state of the road segment, this approach enhances the interpretability of the model and improves its prediction accuracy.

The Bi-LSTM prediction model used in this paper consists of two stages of data input and output, where the input data sets for both stages,  $X_{1i}$  and  $X_{2i}$ , include feature data and destination data. As shown in Fig. 6, in the first stage, the feature data of  $X_{1i}$  include the data  $Q_p, C_p$  and  $t_{fi}$  set for different cycles, as well as the resulting traffic parameter data  $Q_{1p}, Q_{2p}, v_p, k_p$  and  $R_p$ , where  $R_i$  is calculated using formulas (7) and (8). The destination data is the queue length of stranded vehicles  $L_i$  for each cycle, calculated using formula (9), and the output data is the model's predicted queue length of stranded vehicles  $L_j$  for a future cycle. In the second stage, the feature data of  $X_{2i}$  are based on the data from the first stage, excluding  $R_p$ , and further include the predicted  $L_j$  from the first stage model and the occupancy state  $S_{g1p}, S_{g2p}, S_{r1p}$  and  $S_{r2i}$  of detector 1 and detector 2 from Fig. 2. The destination data for this stage is the traffic spillover dissipation state  $P_i$  for each cycle (as derived from Table 1), and the output data is the model's predicted traffic spillover dissipation state  $P_j$  for a future cycle.

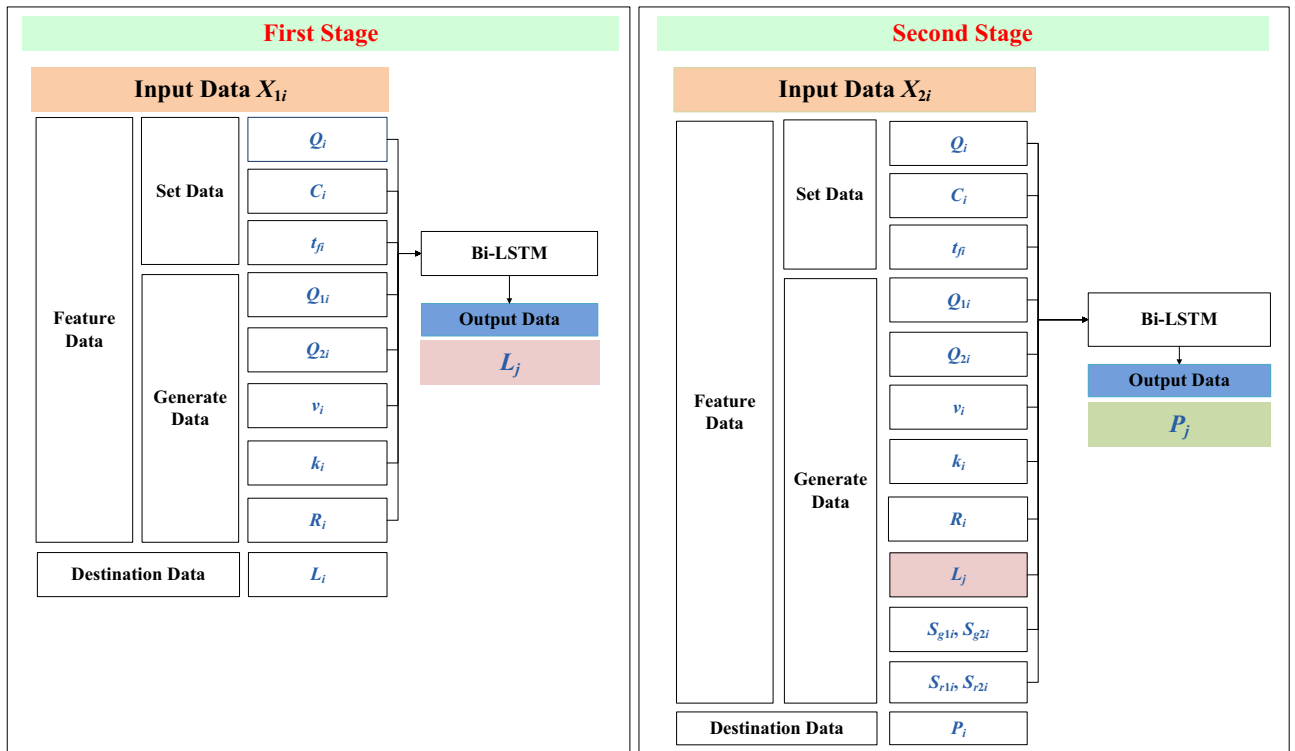


**Fig. 6.** Data input and output of the two-stage prediction model.

*Model training*

Based on the principles of the above Bi-LSTM model and the data input and output, the training process of the Bi-LSTM-based two-stage traffic spillover dissipation prediction model is shown in Fig. 7. The specific process is as follows.

- (1) Data setup: Traffic data for  $N$  cycles is collected using the VISSIM 11 to form the two-stage input data sets  $X_{1i}$  and  $X_{2i}$ . Then, based on the content of Section "Data input and output of the prediction model", the feature data, destination data, and output data in the two-stage prediction model are set, and they are split into training and testing sets at an 8:1 ratio.
- (2) K-fold cross-validation: To ensure the reliability of the model, the dataset is randomly divided into 10 subsets of similar size. Each time, one subset is selected as the test set, and the remaining 9 subsets are used as the training set. This allows for 10 rounds of training and testing, generating 10 model performance metrics. The average and standard deviation of these metrics are then calculated to evaluate the model's stability and generalization ability.
- (3) Hyperparameter tuning: The Random Search method is employed to optimize the hyperparameters of the Bi-LSTM model, such as the number of epochs (training iterations over the entire dataset) and batch size (number of samples per gradient update). Specifically, a predefined number of hyperparameter combinations are randomly sampled from the specified search space. Each combination is used to train the model, and its performance is evaluated on a validation set. The combination yielding the best performance is selected.
- (4) Parameter adjustment: Set the initial parameters of the Bi-LSTM model, and adjust parameters such as *epoch* (number of training samples) and *batch size* through experience and multiple trials, until the adjustment is completed when  $R^2$  is greater than or equal to 0.9.
- (5) Determination of evaluation index: This paper selects commonly used evaluation index for predictive models: Mean Absolute Percentage Error (*MAPE*), Mean Absolute Error (*MAE*), Root Mean Squared Error (*RMSE*), and Coefficient of Determination ( $R^2$ ). However, since the real-world data contains zeros, which would lead to division by zero in *MAPE* calculations, *MAE*, *RMSE*, and  $R^2$  are used as the primary index to assess the regression performance. Specifically, smaller *MAE* and *RMSE* values indicate lower prediction errors, while a larger  $R^2$  value signifies a better fit of the model. The specific formulas are as follows.

$$MAE = \frac{1}{n} \sum_{i=1}^n |y_i - p_i| \in [0, +\infty] \tag{22}$$

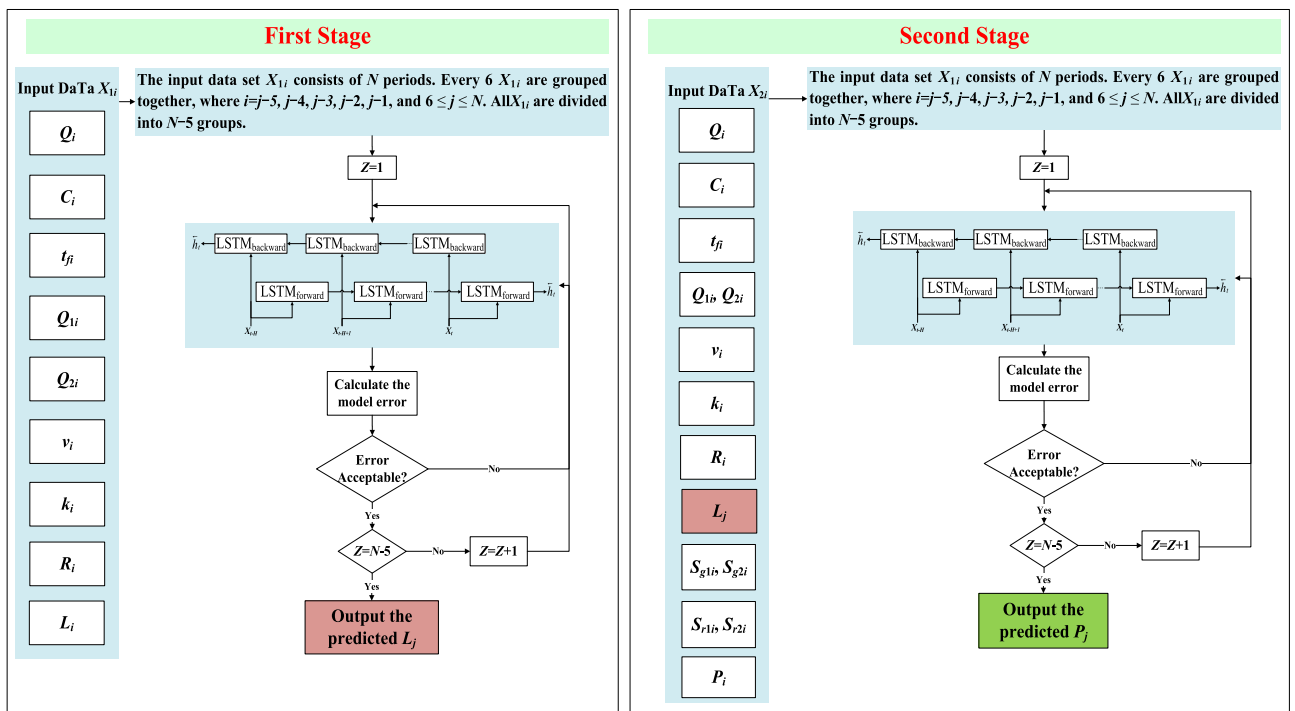


Fig. 7. Bi-LSTM model two-stage training flow chart.

$$R^2 = 1 - \frac{\sum_{i=1}^n (y_i - p_i)^2}{\sum_{i=1}^n (y_i - \bar{y})^2} \in [0, 1] \tag{23}$$

$$RMSE = \sqrt{\frac{1}{n} \sum_{i=1}^n (y_i - p_i)^2} \in [0, +\infty] \tag{24}$$

Where  $n$  is the number of samples,  $y_i$  is the true value of the  $i$ -th sample,  $p_i$  is the predicted value of the  $i$ -th sample, and  $\bar{y}$  is the average of the true values of the samples.

- (6) Data grouping: Since traffic flow has a certain level of continuity, traffic flow characteristics are generally stable over 10 to 15 min. Using a 100-s cycle for measurement, there are 6 cycles in 10 min. Therefore, predicting the destination data for the 6th cycle using the input data from the previous 5 cycles yields good results. Thus, every 6 cycles of input data  $X_{1i}$  or  $X_{2i}$  are grouped together, and each stage is divided into  $N-5$  groups, where  $i$  takes values of  $j-5, j-4, j-3, j-2, j-1$ , with  $6 \leq j \leq N$ , where  $j$  is the cycle number.
- (7) Model training: In the first stage, the grouped  $X_{1i}$  is input into the Bi-LSTM model. The training is done using the data from the first to the fifth cycle of the first input group. After training, the output is compared with the actual data of the 6th cycle. If the model error, measured by  $R^2$  or  $RMSE$ , meets the requirements, the next group of input data is trained. This continues until all  $N-5$  groups of input data have been trained. The model will then output the predicted road segment queue length  $L_j$  for a future cycle. In the second stage, after the model has completed training in the first stage, the output  $L_j$  from the first stage is incorporated as feature data. Similarly, the grouped  $X_{2i}$  is input into the Bi-LSTM model. Training begins with the first input group and continues until all  $N-5$  groups have been trained. The model will then output the predicted road traffic spillover dissipation state  $P_j$  for a future cycle.

Through the above settings of model principles, data input and output, evaluation index, and model training, it is convenient to understand the composition of the two-stage prediction model for traffic spillover dissipation based on Bi-LSTM, providing a theoretical foundation for the construction of subsequent prediction models.

## Results

### Data collection

Set up a short-distance intersection simulation network in the VISSIM 11 as shown in Fig. 8. The segment length  $L$  is 150m, and  $L_s$  is 80m, with the driving direction heading west. Two data collection points and two types of detectors are set up on this section to collect the data required for the prediction model.

The data corresponding to each scenario are collected according to the data collection method described in Section "Data collection approach and methods". Taking one data collection scenario as an example, Scenario 6 is selected for  $Q$ , with a corresponding  $t_j$  of -5 s and  $C$  of 100 s. Partial data obtained from this scenario are shown in Table 3.

### Sensitivity analysis

Results of sensitivity analysis for  $Q$

Using  $Q$  as the factor, the simulation data obtained above is used to calculate the probabilities  $\alpha$  corresponding to each value of  $P_i$  (1, 2, 3, 4) over every 6 cycles, as well as the average values of road section queue length  $L$ , speed  $v$ , and density  $k$ . The sensitivity analysis of  $Q$  to  $P$  is shown in Fig. 9. The sum of the probabilities of  $P_i$  taking

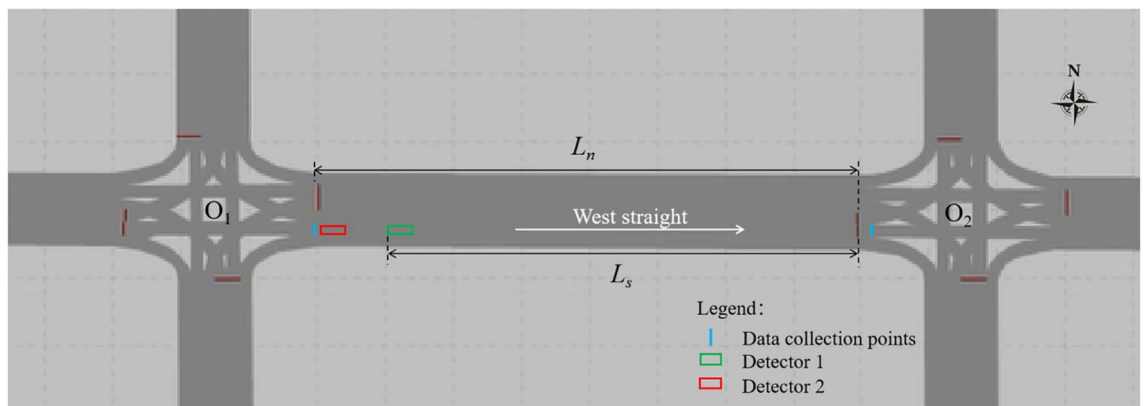


Fig. 8. Short-distance intersection simulation network.

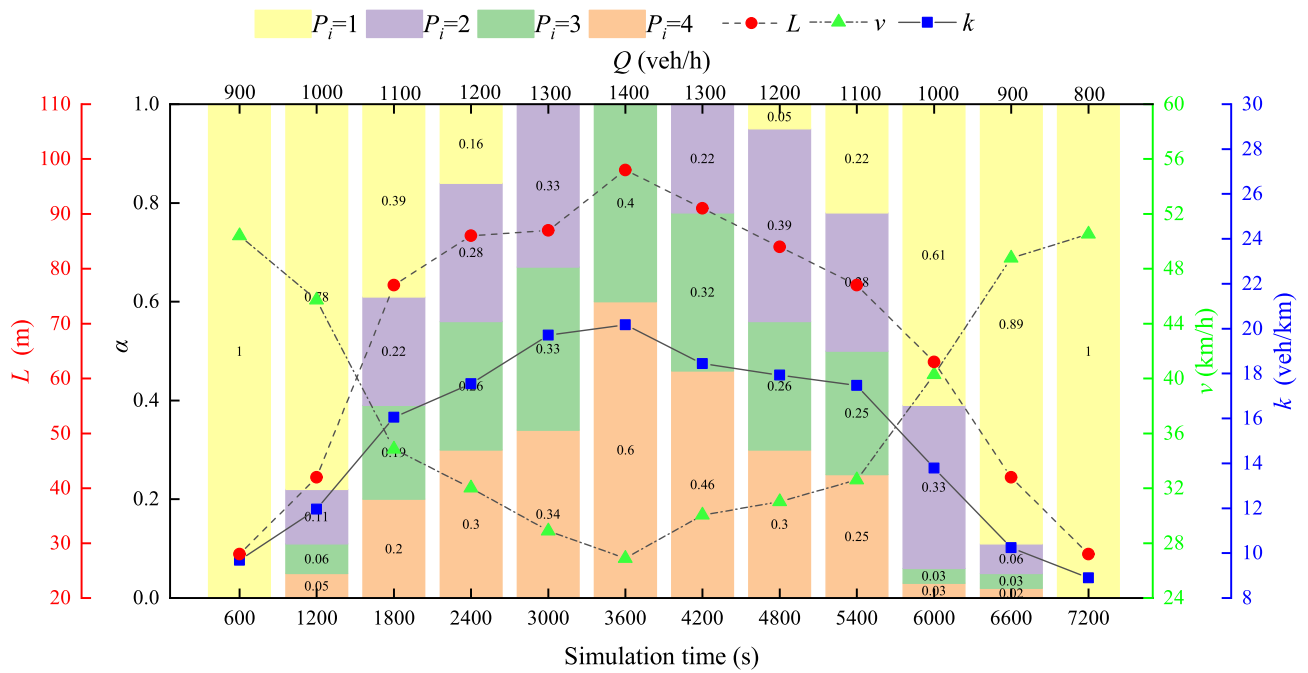


Fig. 9. Sensitivity analysis of  $Q$  with respect to  $P$ .

values 2, 3, and 4 is defined as the probability  $\beta$  of traffic spillover occurring on the road, while the sum of the probabilities of  $P_i$  taking values 3 and 4 is defined as the probability  $\gamma$  of non-dissipating traffic spillover on the road. The correlation analysis of  $Q, L, v, k$  with  $\beta$  and  $\gamma$  is shown in Fig. 10.

As shown in Fig. 9, with the change in the value of  $Q$ ,  $\beta$  generally exhibits a positive correlation and co-variation with  $Q$ . However,  $\beta$  does not change significantly immediately; instead, it changes after  $Q$  increases or decreases to a certain extent. Meanwhile,  $L, v$ , and  $k$  also vary with the value of  $Q$ . At the same time, the larger  $L$  is, the smaller  $v$  is and the larger  $k$  is, the larger  $\beta$  becomes.

As shown in Fig. 10, the correlation coefficient  $R$  between  $Q$  and  $\beta, \gamma$  are approximately 0.95358 and 0.968, respectively; the correlation coefficient  $R$  between  $L$  and  $\beta, \gamma$  are approximately 0.97996 and 0.92704, respectively; the correlation coefficient  $R$  between  $v$  and  $\beta, \gamma$  are approximately -0.99126 and -0.93779, respectively; the correlation coefficient  $R$  between  $k$  and  $\beta, \gamma$  are approximately 0.98969 and 0.94062, respectively. When the number of observed data points  $n=12$ , the correlation coefficient test table<sup>35</sup> shows that  $R_{n-2}=0.576$ . Since the correlation coefficient  $R$  between  $Q, L, k$  and  $\beta, \gamma$  are all positive and above 0.927, which are greater than  $R_{n-2}$ , there is a significant positive correlation between  $Q, L, k$  and  $\beta, \gamma$ . On the other hand, since the correlation coefficient  $R$  between  $v$  and  $\beta, \gamma$  are negative and have absolute values greater than 0.93, which are also greater than  $R_{n-2}$ , there is a significant negative correlation between  $v$  and  $\beta, \gamma$ . This indicates that under the variation of  $Q, L, v$ , and  $k$  all have a significant impact on the traffic spillover dissipation state  $P$  of the road.

Results of sensitivity analysis for  $C$

Using  $C$  as the factor, the simulation data obtained above is used to calculate the probabilities  $\alpha$  for each value of  $P_i$  over 30 cycles, as well as the average values of  $L, v$ , and  $k$ . The sensitivity analysis of  $C$  to  $P$  is shown in Fig. 11. The correlation analysis of  $C, L, v, k$  with  $\beta$  and  $\gamma$  is shown in Fig. 12.

As shown in Fig. 11, with the increase of  $C$ ,  $\beta$  undergoes small fluctuating changes and reaches its minimum at a certain ideal cycle. At the same time, as  $L$  increases,  $v$  decreases, and  $k$  increases,  $\beta$  also increases.

As shown in Fig. 12, the correlation coefficient  $R$  between  $C$  and  $\beta, \gamma$  are approximately -0.67937 and -0.85272, respectively; the correlation coefficient  $R$  between  $L$  and  $\beta, \gamma$  are approximately 0.85326 and 0.72292, respectively; the correlation coefficient  $R$  between  $v$  and  $\beta, \gamma$  are approximately -0.89829 and -0.87268, respectively; the correlation coefficient  $R$  between  $k$  and  $\beta, \gamma$  are approximately 0.90254 and 0.9581, respectively. When the number of observed data points  $n=9$ ,  $R_{n-2}=0.666$ . Since the correlation coefficient  $R$  between  $L$  and  $\beta, \gamma$  are positive and above 0.666, and the correlation coefficient  $R$  between  $k$  and  $\beta, \gamma$  are positive and above 0.902, all of which are greater than  $R_{n-2}$ , there is a positive correlation between  $L$  and  $\beta, \gamma$ , and a significant positive correlation between  $k$  and  $\beta, \gamma$ . Since the correlation coefficient  $R$  between  $C, v$  and  $\beta, \gamma$  are negative and their absolute values are above 0.679, which are also greater than  $R_{n-2}$ , there is a negative correlation between  $C, v$  and  $\beta, \gamma$ . This indicates that under the variation of  $C, L, v$  all have some impact on  $P$ , and  $k$  has a larger impact on  $P$ .

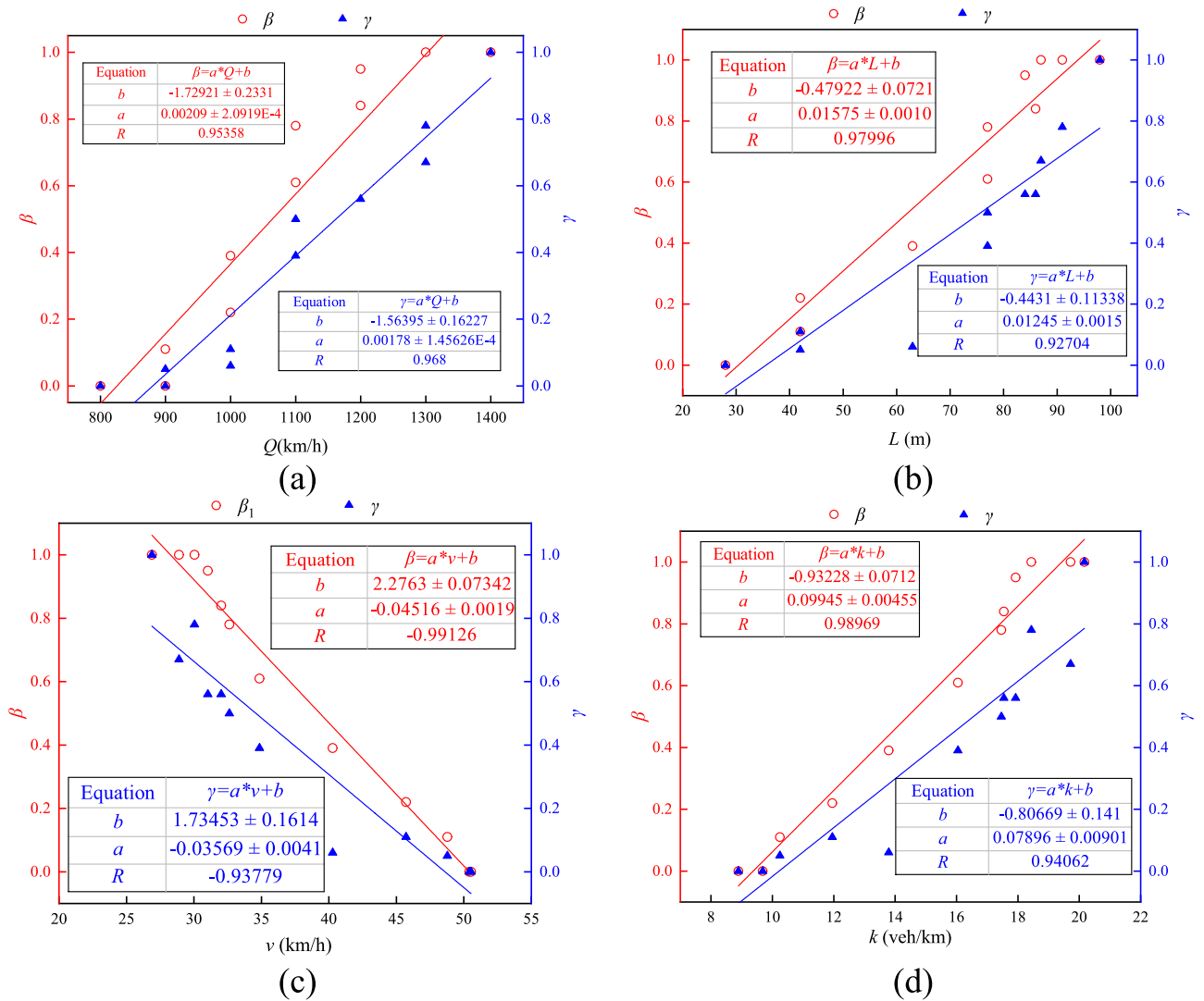


Fig. 10. Correlation analysis of  $Q, L, v, k$  with  $P$ .

Results of sensitivity analysis for  $t_f$

Using  $t_f$  as the factor, the simulation data obtained above is used to calculate the probabilities  $\alpha$  for each value of  $P$  over 36 cycles, as well as the average values of  $L, v,$  and  $k$ . The sensitivity analysis of  $t_f$  to  $P$  is shown in Fig. 13. The correlation analysis of  $t_f, L, v, k$  with  $\beta$  and  $\gamma$  is shown in Fig. 14.

As shown in Fig. 13, with the variation of  $t_f, \beta$  undergoes significant fluctuations and reaches its minimum at a certain ideal offset. At the same time, as  $L$  increases,  $v$  decreases, and  $k$  increases,  $\beta$  also increases.

As shown in Fig. 14, the correlation coefficient  $R$  between  $t_f$  and  $\beta, \gamma$  are approximately 0.69052 and 0.73042, respectively; the correlation coefficient  $R$  between  $L$  and  $\beta, \gamma$  are approximately 0.94465 and 0.93939, respectively; the correlation coefficient  $R$  between  $v$  and  $\beta, \gamma$  are approximately -0.67771 and -0.71087, respectively; the correlation coefficient  $R$  between  $k$  and  $\beta, \gamma$  are approximately 0.68146 and 0.71386, respectively. When the number of observed data points  $n=9, R_{n-2}=0.666$ . Since the correlation coefficient  $R$  between  $t_f$  and  $\beta, \gamma$ , and between  $k$  and  $\beta, \gamma$ , are all positive and above 0.69, and the correlation coefficient  $R$  between  $L$  and  $\beta, \gamma$  are positive and above 0.939, all of which are greater than  $R_{n-2}$ , there is a positive correlation between  $t_f, k$  and  $\beta, \gamma$ , and a significant positive correlation between  $L$  and  $\beta, \gamma$ . Since the correlation coefficient  $R$  between  $v$  and  $\beta, \gamma$  are negative and have absolute values above 0.677, which are also greater than  $R_{n-2}$ , there is a negative correlation between  $v$  and  $\beta, \gamma$ . This indicates that under the variation of  $t_f, t_p, v,$  and  $k$  all have some impact on  $P$ , and  $L$  has a larger impact on  $P$ .

In summary, changes in  $Q, C$  and  $t_f$  affect  $P$  of the road segment, exhibiting a certain causal or correlational relationship. According to the principle that a larger absolute value of the correlation coefficient indicates a closer relationship between features and the target variable,  $Q$  has the highest feature importance. Additionally, the road traffic parameters  $L, v,$  and  $k$  generated during this process also have varying degrees of impact on  $P$ . This further confirms that using the above data as the input for the traffic spillover dissipation prediction model for short-distance intersections proposed in this paper is reasonable.

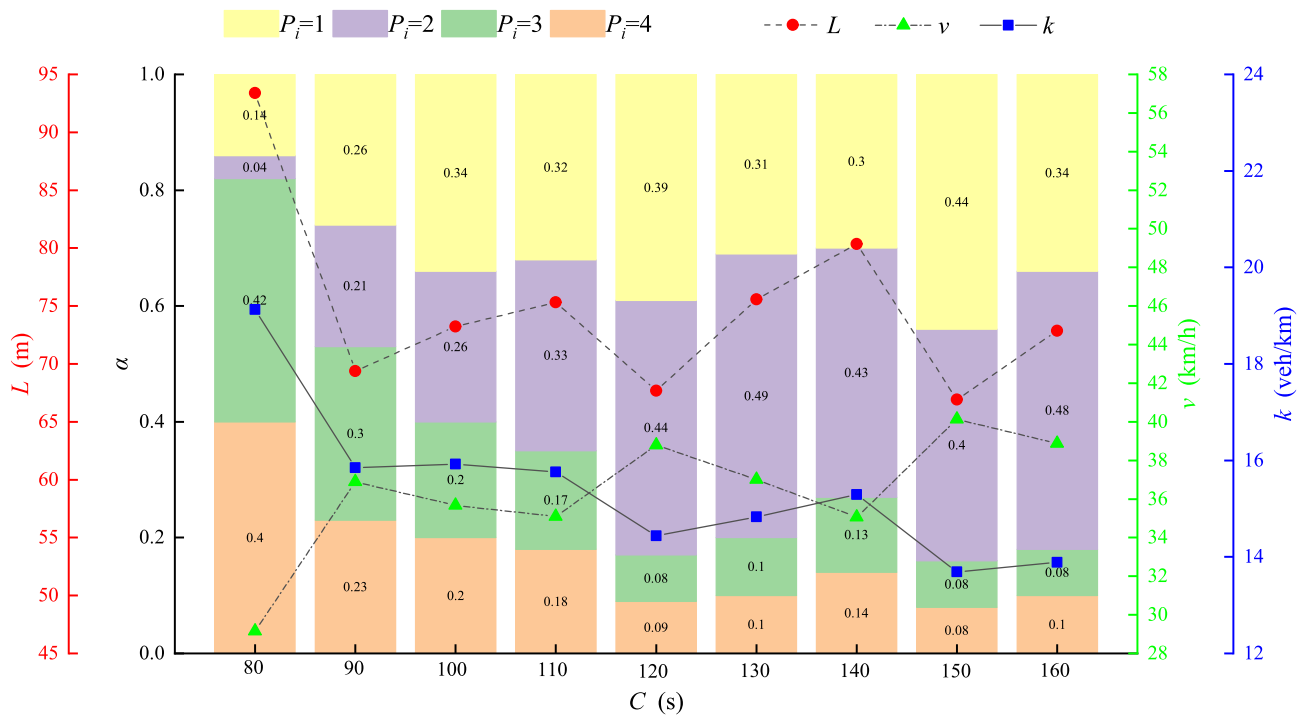


Fig. 11. Sensitivity analysis of C with respect to P.

### Analysis of prediction results

#### Analysis of the prediction model results for queue length of stranded vehicles

In this paper, a traffic spillover dissipation prediction model based on Bi-LSTM is constructed using a Python program according to the content in Sect. "Two-stage prediction model of traffic spillover dissipation based on Bi-LSTM". The first stage of the model prediction is performed using Bi-LSTM, which predicts the queue length of stranded vehicles  $L_j$  in a future cycle. The prediction results are compared with those obtained using other machine learning algorithms such as DT, CNN, RF, LSTM and GRU. Taking  $t_j = -5s$  and  $C = 100s$  as an example, Q is selected from Scheme 1 to 10, and a total of 720 data points are collected. The prediction results and evaluation index of different models are compared and analyzed using 80 corresponding test set data, as shown in Fig. 15 and Table 4.

As shown in Fig. 15, it displays the comparison between the predicted value and true value of the queuing length of stranded vehicles output by each model. However, due to the dense prediction results of each model, a partial line chart is amplified for easy observation. As seen in Fig. 15, compared to the DT, CNN, and RF models, the GRU and LSTM model are more sensitive to time series data, and its predicted results are closer to the true values. Additionally, as shown in Table 4, the  $R^2$ , RMSE, and MAE of the DT model are 0.941, 7.369 and 6.188, respectively; those of the CNN model are 0.949, 6.825 and 5.663, respectively; those of the RF model are 0.956, 6.348 and 5.200, respectively; those of the GRU model are 0.963, 5.942 and 4.800, respectively; and those of the LSTM model are 0.963, 5.831 and 4.725, respectively. Since a larger  $R^2$  indicates a higher model fitting degree, and smaller RMSE and MAE indicate smaller model errors, the fitting degree and error performance of the GRU and LSTM models are superior to those of the DT, CNN and RF models. Additionally, since a larger  $R^2$  indicates a higher model fit and a smaller RMSE indicates smaller model errors, Table 4 shows that the GRU and LSTM model outperform the DT, CNN and RF models in both fit and error. Compared to the LSTM prediction model, the Bi-LSTM model can capture both forward and backward contextual information in the time series data, making it superior to the LSTM model, which can only capture data in a forward direction.

Therefore, it can be seen from Fig. 15 that the prediction results of the Bi-LSTM model are closest to the true values. Meanwhile, as shown in Table 4, the  $R^2$ , RMSE, and MAE of the Bi-LSTM model are 0.968, 5.403, and 4.300, respectively, indicating that the Bi-LSTM model has the highest fitting degree and the smallest prediction error. The above comparison results demonstrate that based on the LSTM model, the further adoption of the Bi-LSTM model to predict the queuing length of stranded vehicles on road segments is effective, and its results are optimal.

To further analyze the prediction accuracy of the above Bi-LSTM model, the predicted values of  $L_j$  output by the Bi-LSTM model were randomly ranked and compared with the true value, and the error distribution map and a unilinear analysis map were plotted, as shown in Fig. 16 and Fig. 17.

In Fig. 16, the blue scatter points represent the predicted values of  $L_j$  from the model's test set, while the green bands indicate the error distribution between the predicted and actual values of  $L_j$ . A narrower green band signifies a smaller prediction error; for instance, the error for the first 0–11 data points is zero. As  $L_j$  increases, errors emerge, yet the difference between the predicted and actual values of  $L_j$  does not exceed 9m, with a

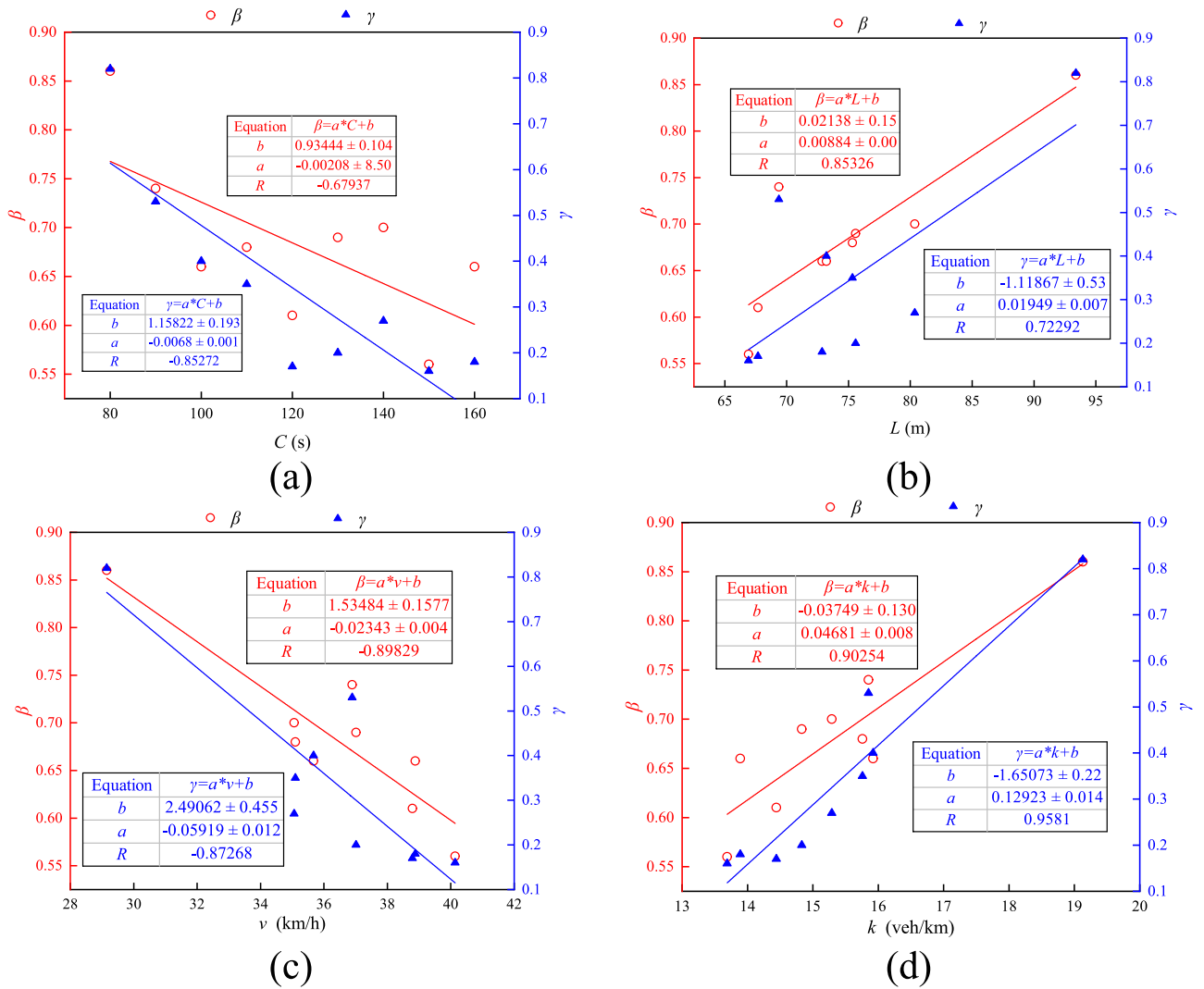


**Fig. 12.** Correlation analysis of  $C, L, v, k$  with  $P$ .

maximum error rate of 14.29%. According to statistics, the average error rate between the predicted and actual values of  $L_j$  is 6.6%. As illustrated in Fig. 17, the equation  $y = 0.992x + 0.517$  represents the fitting straight line function between the predicted and actual values of  $L_j$ . The slope  $k$  of  $x$  is 0.992, and the intercept  $b$  is 0.517. The closer the slope  $k$  is to 1 and the intercept  $b$  is to 0, the closer the fitting line is to  $y = x$ , indicating that the true values and predicted values are closer. Therefore, through the above analysis, it can be concluded that the two-stage traffic spillover dissipation prediction model based on Bi-LSTM proposed in this paper has high accuracy in predicting the road queue length of stranded vehicles in the first stage.

*Analysis of the traffic spillover dissipation prediction model results*

Based on the completion of the first stage of the model prediction, the predicted  $L_j$  from the first stage is used as feature data for the second stage, continuing with the prediction for the second stage, i.e., predicting the traffic spillover dissipation state  $P_j$  for a future cycle. To better validate the effectiveness of the two-stage traffic spillover dissipation prediction model based on Bi-LSTM proposed in this paper, a single-stage traffic spillover dissipation prediction model was also set up. In this model, after inputting feature and destination data, the model can directly predict  $P_j$  without using the  $L_j$  predicted in the first stage as feature data for the second stage. The prediction results and evaluation index of this model are compared with those of the two-stage prediction model, as shown in Fig. 18 and Table 5, where the test data is randomly selected from 800 data points from the test set corresponding to all collected data.

Figure 18 records the prediction scenarios of the single-stage model and the two-stage model, where  $x-y$  indicates that when the true value of  $P_j$  is  $x$ , the predicted value output by the model is  $y$ . Since  $P_j$  has four possible prediction outcomes:  $P_j = 1$  (no traffic spillover),  $P_j = 2$  (effectively dissipating traffic spillover),  $P_j = 3$  (potentially non-dissipating traffic spillover), and  $P_j = 4$  (absolutely non-dissipating traffic spillover), both  $x$  and  $y$  can take values of 1, 2, 3, or 4, resulting in 16 possible prediction scenarios: 1-1, 1-2, 1-3, 1-4, 2-1, 2-2, 2-3, 2-4, 3-1, 3-2, 3-3, 3-4, 4-1, 4-2, 4-3, and 4-4. However, only 9 scenarios are included in the randomly selected

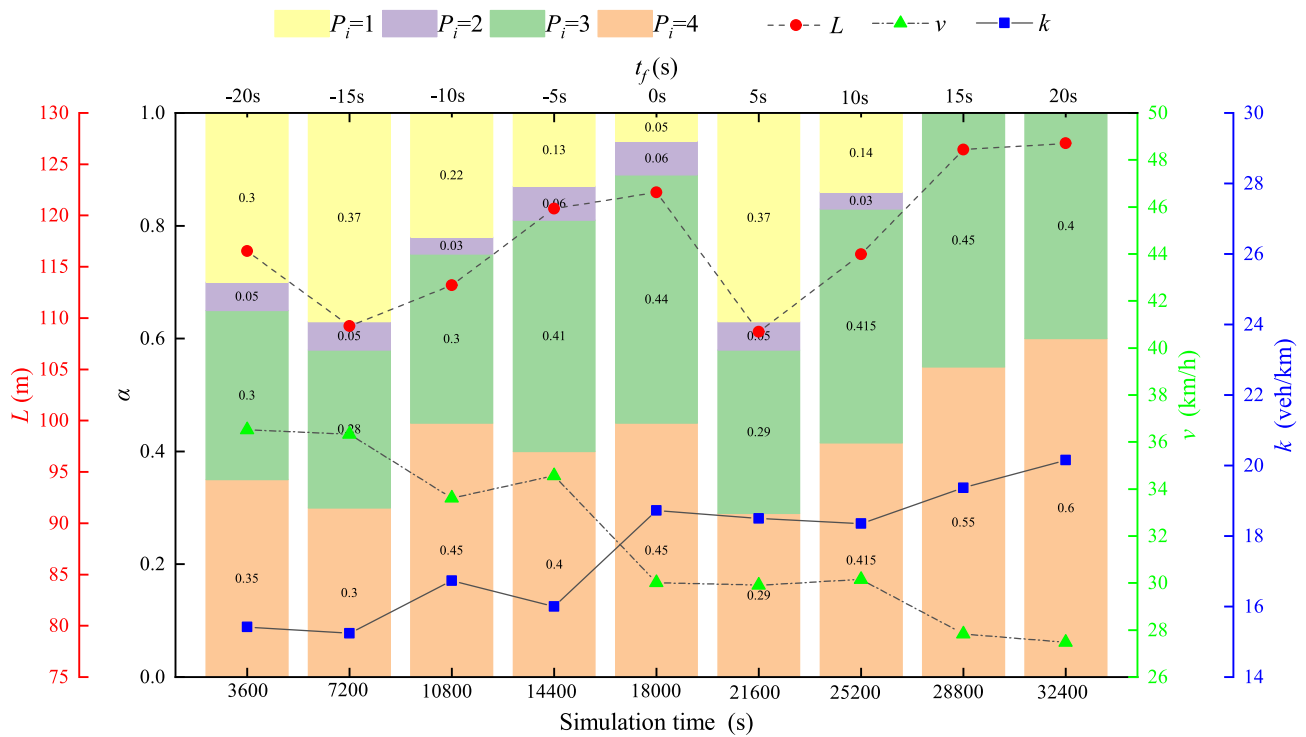


Fig. 13. Sensitivity analysis of  $t_f$  with respect to  $P$ .

800 pieces of data. For the single-stage prediction model, the scenarios of 1-1, 2-2, 3-3, 4-4, 1-2, 2-1, 3-2, 3-4, and 4-3 occurred 279 times, 117 times, 128 times, 162 times, 26 times, 35 times, 13 times, 10 times, and 30 times, respectively. For the two-stage prediction model, these scenarios occurred 294 times, 132 times, 141 times, 176 times, 11 times, 20 times, 8 times, 2 times, and 16 times, respectively. Statistically, the accuracy of traffic spillover identification for the single-stage and two-stage prediction models (the accuracy when  $P_j$  takes the values of 1, 2, 3, and 4) is 85.75% and 92.88%, respectively. The accuracy of traffic spillover dissipation prediction (the accuracy when  $P_j$  takes the values of 2, 3, and 4) is 82.88% and 90.71%, respectively. As shown in Table 5, the  $R^2$ ,  $RMSE$  and  $MAE$  for the single-stage prediction model are 0.901, 0.377 and 0.138, respectively, while the  $R^2$ ,  $RMSE$  and  $MAE$  for the two-stage prediction model are 0.951, 0.267 and 0.075, respectively. The above comparison results show that the two-stage prediction model is superior and is an effective improvement over the single-stage prediction model.

To further analyze the model's prediction performance in different traffic flow intervals, we continue using  $t_f = -5s$  and  $C = 100s$  as examples. The  $Q$  values are selected from schemes 1 to 10, and a total of 720 data points are collected. From these, 80 data points are randomly selected from the following 8 traffic flow intervals: [725,900], (900,1000], (1000,1100], (1100,1200], (1200,1300], (1300,1400], (1400,1500], and (1500,1575], with 10 data points selected from each interval for testing. The prediction results for each flow interval are shown in Fig. 19.

As shown in Fig. 19, it displays the comparison between the true values of  $P_j$  in different traffic flow intervals and the predicted values from the single-stage model and the two-stage model. Red circles indicate where prediction deviations exist. As shown in Fig. 19, compared to the single-stage prediction model, the two-stage prediction model provides more accurate results with less deviation. Except for the traffic flow intervals of (1100,1200], (1200,1300], and (1300,1400], where a few predicted values do not match the true values, the predicted values for all other flow intervals are identical to the true values.

To further analyze the relationship between the predicted values of  $P_j$  in the second stage of the two-stage prediction model and the true values, the true and predicted values corresponding to different traffic flow intervals in Fig. 19 are recorded. The occurrence times of different scenarios is then statistically analyzed, as shown in Fig. 20. In Fig. 20, the colors for 1-1, 2-2, 3-3, and 4-4 are all in the green range, indicating accurate predictions; the colors for 2-1 and 4-3 are in the purple range, indicating deviations in the predictions. Other scenarios with a time of 0 are not displayed in the figure.

As shown in Fig. 20, the entire traffic flow interval can be divided into three stages. Stage 1 and Stage 3 both have accurate predictions, while Stage 2 has 3 instances of inaccurate predictions. A detailed analysis is as follows.

Stage 1: When the traffic flow is in the [725,900] and (900,1000] intervals, the flow is relatively low, with no traffic spillover occurring, and the traffic flow is quite stable. The prediction model can accurately predict the state of no traffic spillover on the road, with no prediction errors.

Stage 2: When the traffic flow gradually increases, the number of traffic spillover occurrences on road segments in the flow intervals of (1100, 1200], (1200, 1300], and (1300, 1400] begins to increase continuously, leading to some critical situations. For example, when the upstream intersection has a green light, if detector 1 is

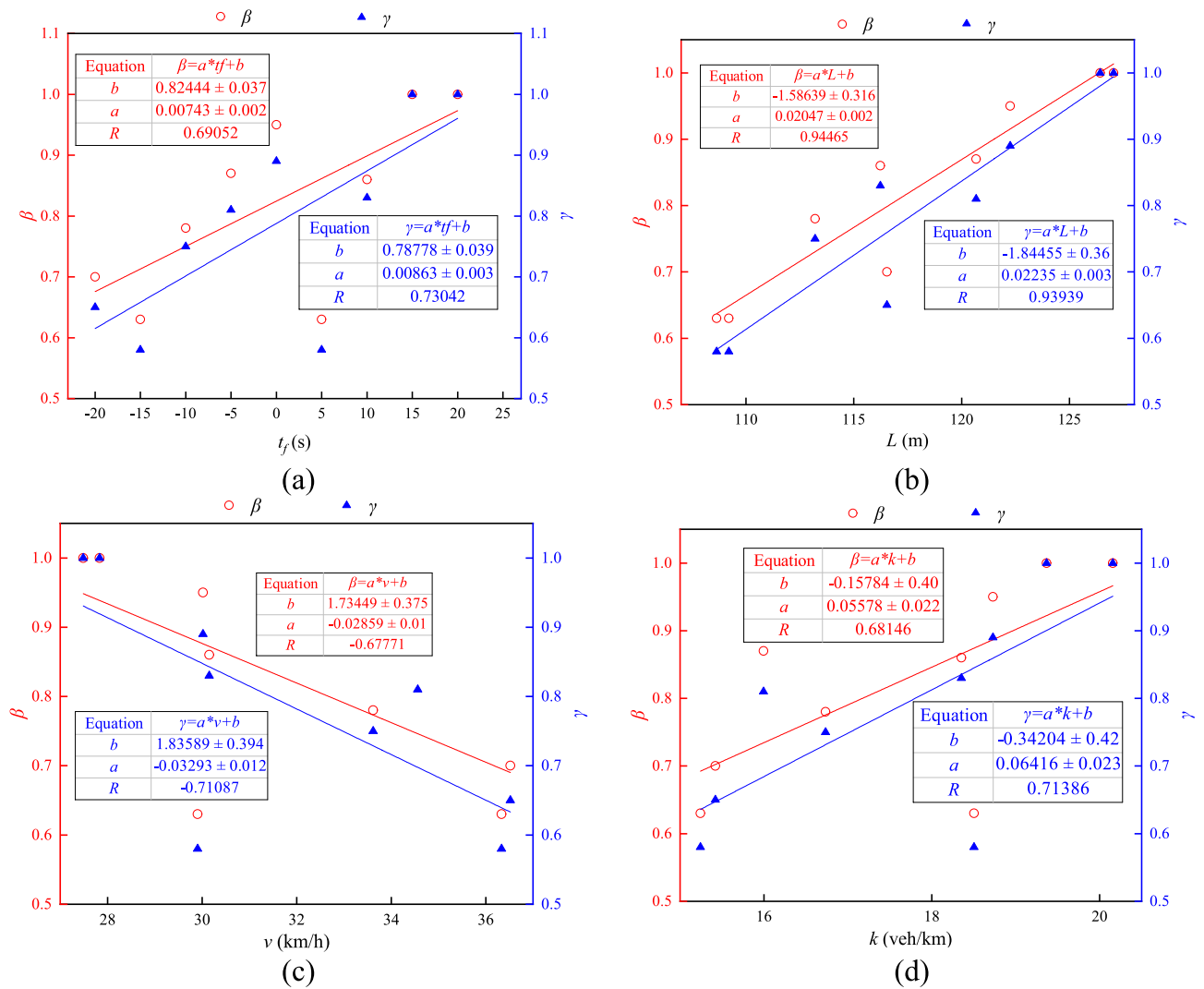


**Fig. 14.** Correlation analysis of  $t_p$ ,  $L$ ,  $v$ ,  $k$  with  $P$ .

occupied and the tail of the queuing vehicles on the road segment is near detector 2,  $P_i$  may be detected as 1 or 2; when the upstream intersection has a red light, if detector 1 is occupied and the tail of the queuing vehicles is near detector 2,  $P_i$  may be detected as 3 or 4 (as shown in Fig. 21), with the corresponding prediction scenario being 4–3. In this stage, the prediction results for traffic spillover dissipation are not completely accurate, but such deviations occur infrequently and have a negligible impact on the overall prediction results.

Stage 3: When the flow increases to the (1400, 1500] and [1500, 1600] intervals, the number of instances of traffic spillover that cannot dissipate in time increases significantly, while the number of instances with no traffic spillover decreases sharply. In this stage, the traffic spillover state recognition reaches a stable state, and the prediction model can accurately predict whether traffic spillover will occur in a given future period, as well as whether the spillover will dissipate in time, without any prediction deviation.

The model prediction results are verified through simulation. Taking  $t_f = -10s$ ,  $C = 100s$ , and  $Q$  using Scheme 1 as an example, the traffic spillover dissipation state for the 33rd period is predicted, with data from periods 28 to 32 used as input. The model predicts that the traffic spillover in the 33rd period will dissipate effectively (i.e.,  $P_j = 2$ ), and in the actual simulation, the traffic spillover in the 33rd period also dissipates effectively, as shown in Figs. 22 and 23. In Fig. 22, traffic spillover occurs during the green light time for westbound traffic at the upstream intersection, and in Fig. 23, when the red light for westbound traffic begins at the upstream intersection, the queuing vehicles are within the safe distance, indicating that the traffic spillover can dissipate in time. Through validation using the VISSIM 11, the effectiveness of the two-stage traffic spillover dissipation prediction model for short-distance intersections proposed in this paper is further confirmed.

### Discussion

In terms of data collection, the traffic spillover identification and dissipation judgment conditions for short-distance intersections are proposed combined with traffic wave theory. Based on this, VISSIM 11 is used to construct simulation road networks for two short-distance intersections. By setting different input  $Q$ ,  $C$ , and

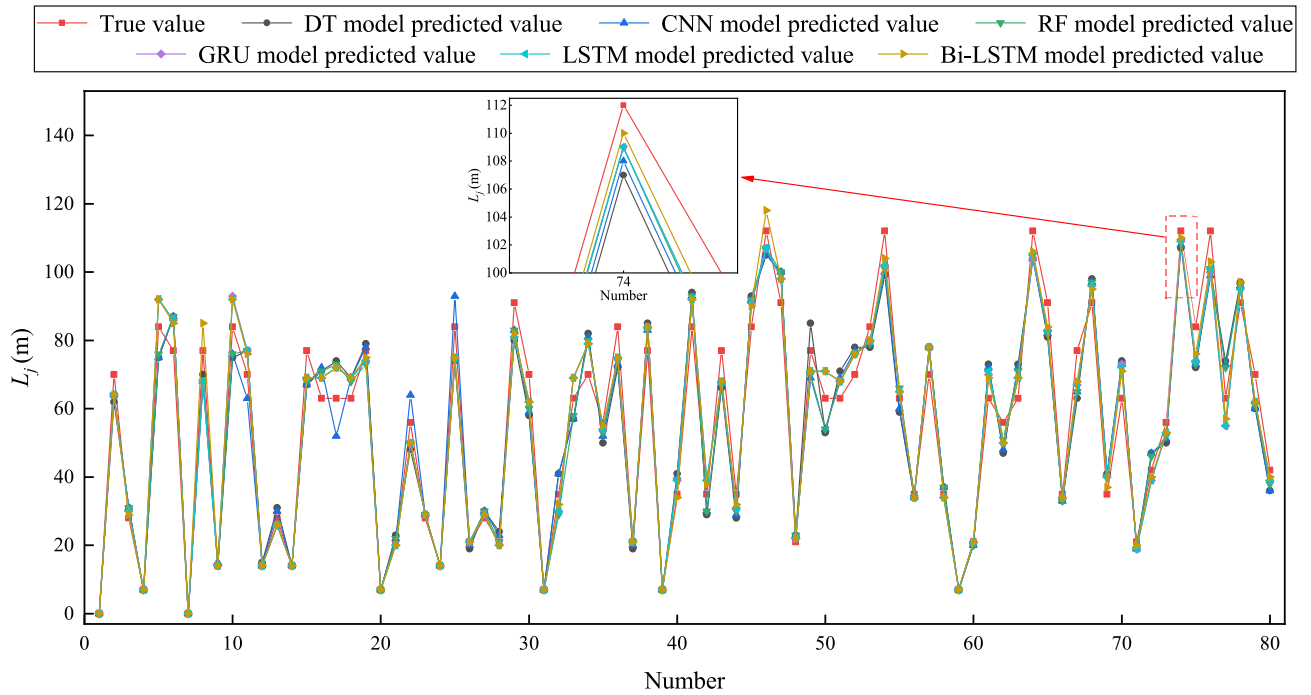


Fig. 15. Comparison of prediction results from different models.

| Model | DT    | CNN   | RF    | GRU   | LSTM  | Bi-LSTM |
|-------|-------|-------|-------|-------|-------|---------|
| $R^2$ | 0.941 | 0.949 | 0.956 | 0.962 | 0.963 | 0.968   |
| RMSE  | 7.369 | 6.825 | 6.348 | 5.942 | 5.831 | 5.403   |
| MAE   | 6.188 | 5.663 | 5.200 | 4.800 | 4.725 | 4.300   |

Table 4. Comparison of evaluation index for different models.

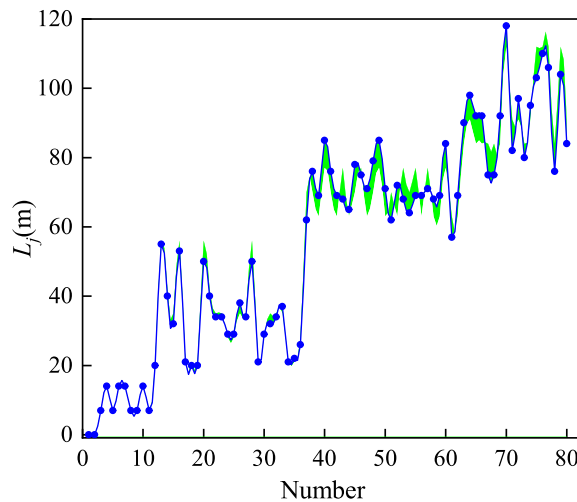


Fig. 16. Predictive value and error distribution.

$t_i$  corresponding to different data collection schemes, data such as the number of  $Q_{1i}$ ,  $Q_{2i}$ ,  $R_i$ ,  $L_i$ ,  $v_i$ ,  $k_i$ ,  $S_{g1i}$ ,  $S_{g2i}$ ,  $S_{r1i}$  and  $S_{r2i}$ , and  $P_i$  for each cycle were obtained. Machine learning models are then used to predict traffic spillover dissipation between road at short-distance intersections, which helps improve the interpretability of the prediction model.

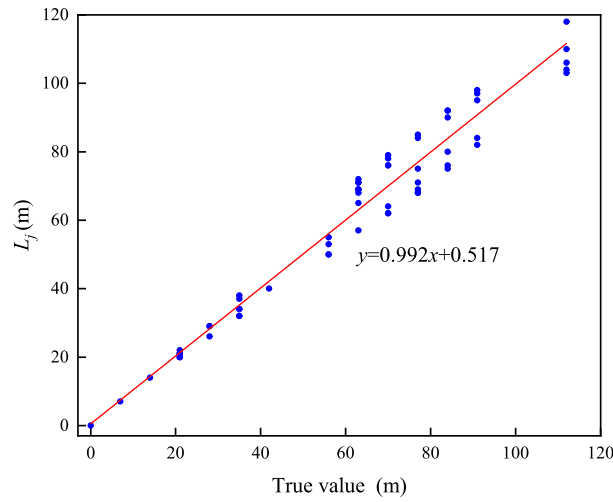


Fig. 17. Unitary linear analysis.

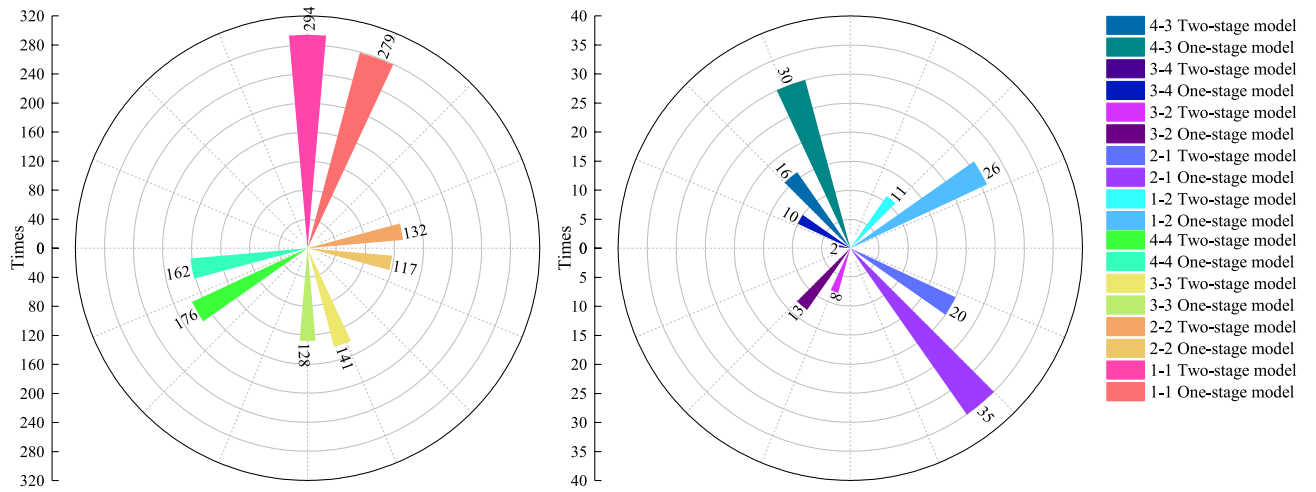


Fig. 18. Comparison of prediction results between single-stage and two-stage prediction models.

|       | Single-stage prediction | Two-stage prediction |
|-------|-------------------------|----------------------|
| $R^2$ | 0.901                   | 0.951                |
| RMSE  | 0.377                   | 0.267                |
| MAE   | 0.138                   | 0.075                |

Table 5. Comparison of evaluation index between single-stage and two-stage prediction models.

In terms of the feasibility verification of the Bi-LSTM model selection, we construct six machine learning models—DT, CNN, RF, GRU, LSTM and Bi-LSTM—using Python to predict the queue length of stranded vehicles ( $L_j$ ) for a future cycle in the first stage, followed by a comparative analysis. The results show that the GRU and LSTM model, which are more sensitive to time series data, outperforms the DT, CNN, and RF models. Compared with the DT, CNN and RF models, the MAE of the LSTM model decreased by 23.64%, 16.56% and 9.13%, respectively; the RMSE decreased by 20.87%, 14.56% and 8.14%, respectively; and the  $R^2$  increased by 2.34%, 1.48% and 0.73%, respectively. For the GRU model, the MAE decreased by 22.43%, 15.24%, and 7.69%, respectively; the RMSE decreased by 19.36%, 12.94% and 6.40%, respectively; and the  $R^2$  increased by 2.23%, 1.48%, and 1.26%, respectively. Although the MAE, RMSE and  $R^2$  values of the GRU and LSTM models are quite close, the LSTM model slightly outperforms the GRU model. The Bi-LSTM model, which can capture contextual information of time-series data in both forward and backward directions, outperforms the GRU and LSTM models that can only capture data in the forward direction. Compared with the GRU and LSTM models,

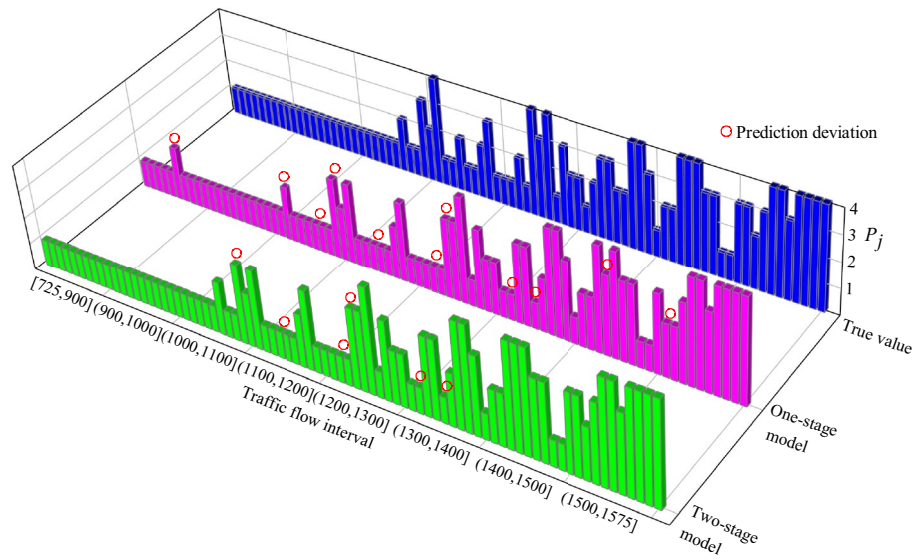


Fig. 19. Prediction results of single-stage and two-stage models in different traffic flow intervals.

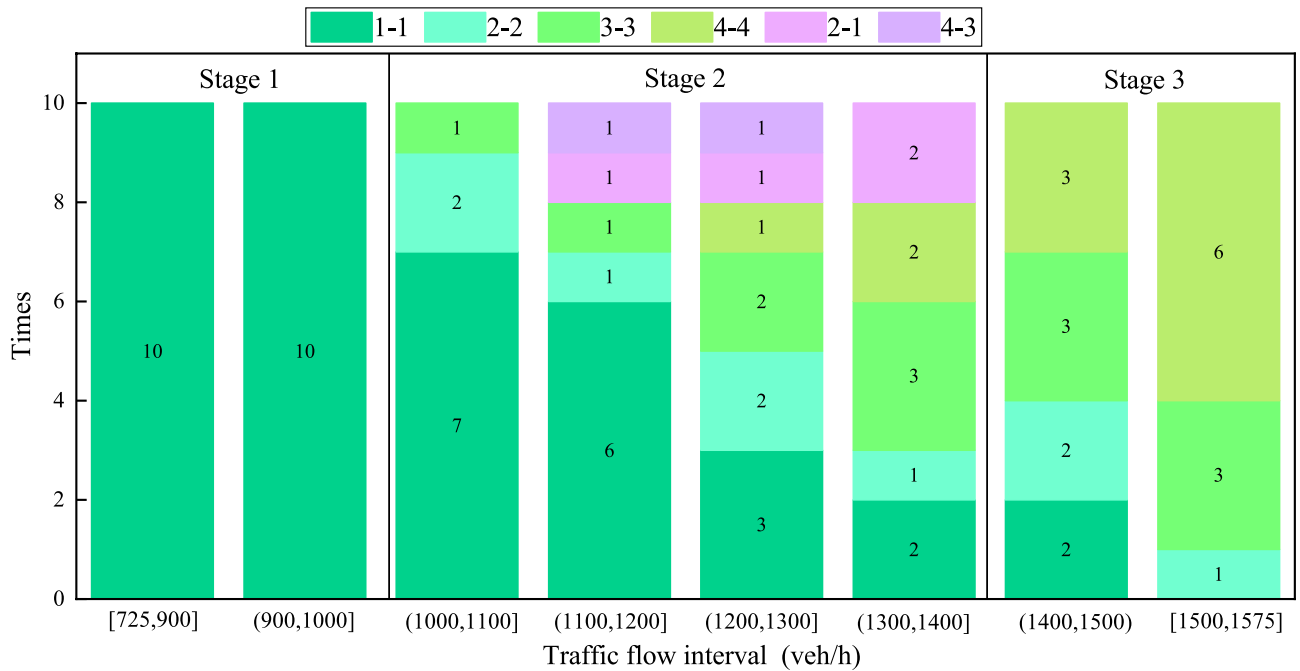


Fig. 20. Analysis of prediction scenarios in different traffic flow intervals.

its MAE decreases by 10.42% and 8.99%, respectively; the RMSE decreases by 9.07% and 7.34%, respectively; and the  $R^2$  increases by 0.62% and 0.52%, respectively. This indicates that the Bi-LSTM model has higher prediction accuracy, and it is feasible to use the Bi-LSTM model in this study to predict traffic spillover dissipation at short-distance intersections. Compared with Reference<sup>18</sup>, which estimates the queuing length under spillover conditions based on low-resolution detector data with an average error rate of 14.9% (prediction accuracy of 85.1%), and Reference<sup>15</sup>, which first predicts traffic flow and then uses the predicted flow in a queue length calculation model to obtain real-time prediction with an average error rate of 14.2% (prediction accuracy of 85.8%), this study uses traffic wave theory and the initial stranded vehicle queue length formula to identify traffic parameters related to road segment queue length, and collects these parameters as inputs to the prediction model. This improves the interpretability of the prediction model. Therefore, the average error rate of the road segment stranded vehicle queue length predicted by the Bi-LSTM model in the first stage is reduced to 14.2% (prediction accuracy of 85.8%), and the model can predict queue length both under non-spillover and spillover conditions. These results indicate that the Bi-LSTM model used in this paper meets the accuracy requirements

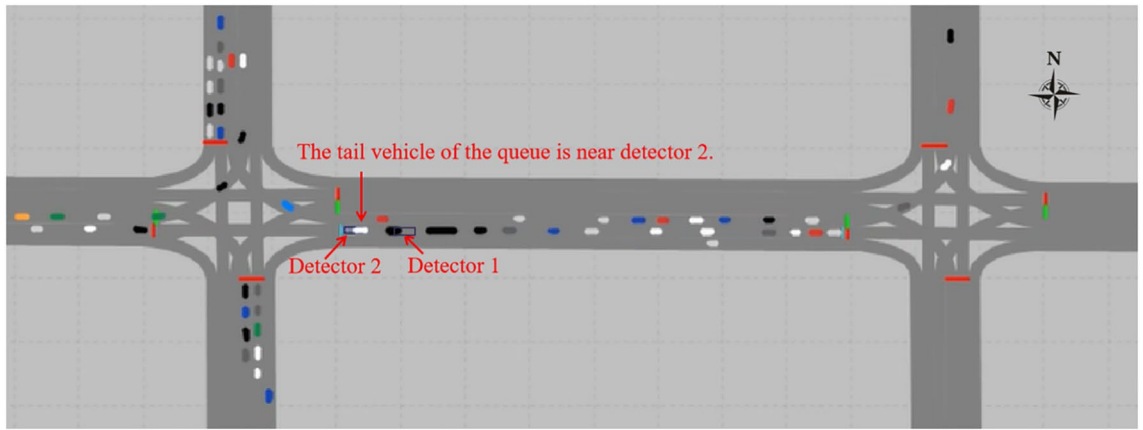


Fig. 21. Simulation scenario corresponding to the prediction case of 4–3.

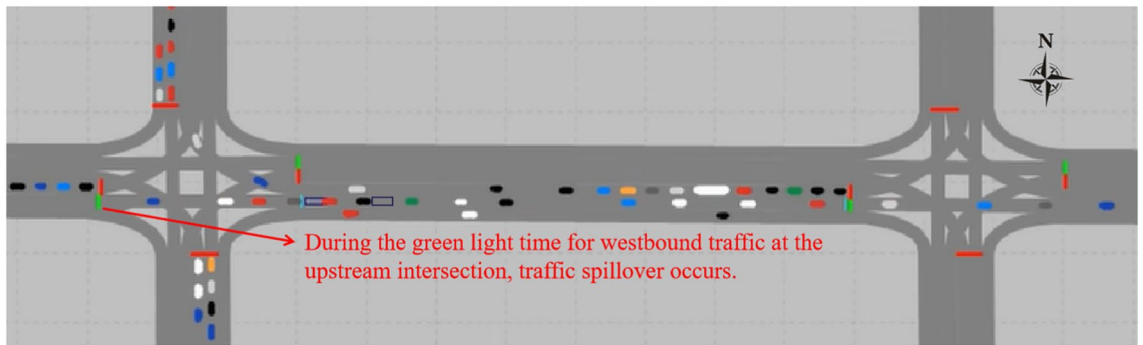


Fig. 22. Traffic spillover occurs during the green light time for westbound traffic at the upstream intersection.

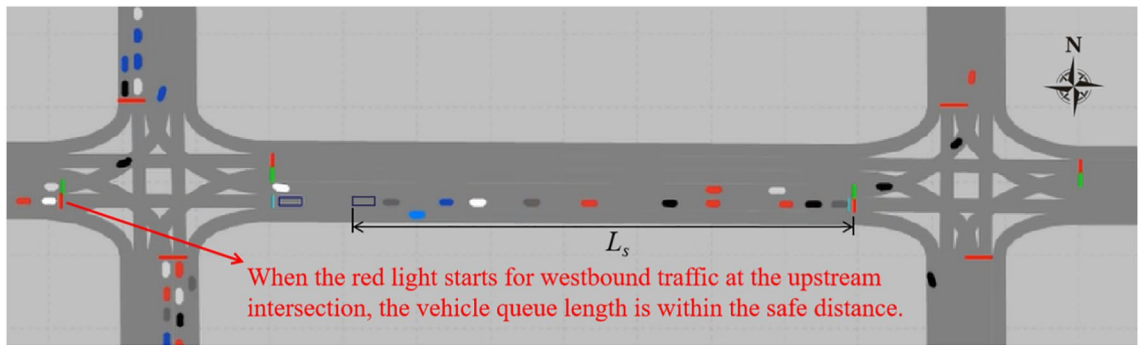


Fig. 23. Traffic spillover dissipates when the red light starts for westbound traffic at the upstream intersection.

for predicting the queue length of stranded vehicles in the first stage and provides a solid foundation for the subsequent prediction of road traffic spillover dissipation.

Building on this, a two-stage prediction method for traffic spillover dissipation based on Bi-LSTM is proposed, where the  $L_j$  predicted in the first stage is used as one of the feature data inputs for the second stage to further predict the traffic spillover dissipation state  $P_j$  for a future cycle at short-distance intersections. To verify the effectiveness of the two-stage prediction method, both a single-stage prediction model and a two-stage prediction model are constructed to predict  $P_j$ . The results show that compared with the single-stage prediction model, the MAE of the two-stage prediction model is reduced by 45.45%, the RMSE is reduced by 29.18%, and the  $R^2$  is increased by 5.55%. This indicates that the evaluation index of the two-stage prediction model are all superior to those of the single-stage prediction model, verifying that the two-stage prediction model proposed in this paper is conducive to further improving the prediction accuracy of  $P_j$ . Compared with the method proposed in reference<sup>7</sup> for identifying traffic spillover through upstream fixed detector occupancy

data, which was verified by simulation to have a spillover identification accuracy rate of 90.45%, this study sets two-stage data input and output based on traffic wave theory, detector data, and sensitivity analysis, enhancing the interpretability of the model. The proposed two-stage traffic spillover dissipation prediction model based on Bi-LSTM can both identify traffic spillover and predict traffic spillover and its dissipation state. The model achieves an accuracy rate of 92.88% in traffic spillover identification and 90.72% in traffic spillover dissipation state prediction, demonstrating good prediction accuracy. It effectively realizes traffic spillover identification and dissipation prediction, which can provide more targeted optimization and control strategies for traffic spillover problems at short-distance intersections and help improve the traffic capacity of short-distance intersections.

## Conclusions

Focusing on the issue of traffic spillover that is often ignored in current studies, particularly the problem where traffic spillover can dissipate on its own, this paper conducts research on traffic spillover dissipation prediction at short-distance intersections. First, the conditions for identifying traffic spillover and determining dissipation at short-distance intersections are proposed combined with traffic wave theory. Based on this, the VISSIM 11 is used to construct traffic operation and data collection scenarios for short-distance intersections. Next, the necessary input data for the prediction model is collected and obtained using methods to calculate the length of vehicle queuing and the traffic spillover dissipation state of the road segments, thus improving the interpretability of the model. Finally, a two-stage traffic spillover dissipation prediction model is constructed using the Bi-LSTM model. The first stage's predicted vehicle queue length is used as feature data for the second stage, effectively improving the model's prediction accuracy. The results show that the model constructed using Bi-LSTM outperforms DT, CNN, RF, GRU and LSTM models in predicting the vehicle queue length in the first stage, with a prediction accuracy of 93.4%, validating the feasibility of selecting the Bi-LSTM model. In the second stage, the model's predictions for the road segment's traffic spillover dissipation state outperform the single-stage prediction model. The model achieves an accuracy of 92.88% in traffic spillover identification and 90.72% in traffic spillover dissipation state prediction, confirming that the proposed two-stage Bi-LSTM model for traffic spillover dissipation is effective and can further improve prediction accuracy. The proposed prediction method can identify traffic spillover at short-distance intersections in advance and, based on this, further predict whether the spillover can dissipate in time. This approach is helpful for selecting targeted signal control strategies to solve the traffic spillover issue at short-distance intersections, thereby effectively improving the traffic capacity of such intersections.

Due to conditional limitations, this study is based on data collected in a traffic simulation environment. The performance of the prediction model when applied to real-world traffic data with more noise and variability remains to be further tested and validated. Therefore, follow-up research will further explore how to adapt to noise in real-world traffic data, how to integrate other data sources (such as weather, socioeconomic data or public transportation schedules) into the model to improve prediction performance, how to integrate the model into existing traffic management systems, how to enhance the model's generalization and scalability, and how to apply it to more traffic scenarios—ultimately extending to practical application scenarios. Additionally, considerations will include the impact of local adjustments on the overall network, the influence of adversarial manipulation, and applications in different cities or countries with varying traffic behaviors and infrastructure designs. In the future, this study will further consider emerging models such as Transformer<sup>37</sup> to enhance the ability to capture global information, address more complex traffic scenarios and task requirements, and continuously improve model performance.

In the future, we will also actively collect real-world traffic data including the behavioral characteristics of emergency vehicles, pedestrians, and vulnerable road users, as well as sudden accident data, to supplement the model. Additionally, we will introduce simulation data of more complex scenarios for model training to enhance the model's adaptability and robustness, while formulating specialized emergency response mechanisms.

In addition, we will further conduct in-depth analyses of scenarios where the model performs poorly. By optimizing the model structure, increasing training with more real-world scenario data, and other means, we will improve the model's prediction accuracy in complex situations, reduce the risks associated with model failure, and ensure the reliability and safety of the model in traffic management.

## Data availability

Data sets generated during the current study are available from the corresponding author on reasonable request.

Received: 15 January 2025; Accepted: 11 June 2025

Published online: 01 July 2025

## References

- Xu, Q. & Zhao, C. Signal optimal control of short-distance intersections on urban arteries. *J. Traffic Transport. Eng.* **39**(01), 91–99 (2023).
- Gazis, D. C. Optimum control of a system of oversaturated intersections. *Oper. Res.* **12**(6), 815–831 (1964).
- Shi, X. W. et al. Modeling for traffic overflow mechanism and its simulation on urban arterial road. *J. Shandong Univ. (Eng. Sci.)* **43**(03), 43–48 (2013).
- Ren, Y. et al. An adaptive signal control scheme to prevent intersection traffic blockage. *IEEE Trans. Intell. Transp. Syst.* **18**(6), 1519–1528 (2016).
- Yang, X. F. et al. Research on urban intersections improvement based on anti-control of traffic spillover. *Highway* **62**(12), 182–187 (2017).
- Zhang, L. D., Jia, L. & Zhu, W. X. Traffic spillover identification based on fuzzy theory. *J. Comput. Appl.* **32**(08), 2378–2380 (2012).
- Ma, D. et al. Identification of spillovers in urban street networks based on upstream fixed traffic data. *KSCE J. Civ. Eng.* **18**, 1539–1547 (2014).

8. Zhu, R. W., Wu, D. & Yang, Z. Triggering conditions and scheme design of queuing overflow control at signalized intersections. *J. Wuhan Univ. Technol. (Transport. Sci. Eng.)* **42**(06), 971–976 (2018).
9. Zhang, L., Zhao, Q. & Wang, L. Research on intersection frequent overflow control strategy based on wide-area radar data. *J. Adv. Transp.* **2020**(1), 9564329 (2020).
10. Wang, J. et al. A signal optimization model of adjacent closely spaced intersections which optimizes pedestrian crossing. *J. Adv. Transp.* **2023**(1), 3964616 (2023).
11. Lee, S., Xie, K., Ngoduy, D. & Keyvan-Ekbatani, M. An advanced deep learning approach to real-time estimation of lane-based queue lengths at a signalized junction. *Transport. Res. Part C: Emerg. Technol.* **109**, 117–136 (2019).
12. Rahman, R. & Hasan, S. Real-time signal queue length prediction using long short-term memory neural network. *Neural Comput. Appl.* **33**, 3311–3324 (2021).
13. Comert, G. et al. Grey models for short-term queue length predictions for adaptive traffic signal control. *Expert Syst. Appl.* **185**, 115618 (2021).
14. Comert, G. & Cetin, M. Queue length estimation from connected vehicles with range measurement sensors at traffic signals. *Appl. Math. Model.* **99**, 418–434 (2021).
15. Dai, L. L., Jiang, G. Y. & Pei, Y. L. Prediction of queue length at saturate signalized intersection. *J. Jilin Univ. (Eng. Technol. Ed.)* **6**, 1287–1290 (2008).
16. Liu, H. X. et al. Real-time queue length estimation for congested signalized intersections. *Transport. Res. part C Emerg. Technol.* **17**(4), 412–427 (2009).
17. Abewickrema, W., Yildirimoglu, M. & Kim, J. Multivariate time-varying Kalman filter approach for cycle-based maximum queue length estimation. *Transport. Res. Part C: Emerg. Technol.* **154**, 104238 (2023).
18. Yao, J. & Tang, K. Cycle-based queue length estimation considering spillover conditions based on low-resolution point detector data. *Transport. Res. part C: Emerg. Technol.* **109**, 1–18 (2019).
19. Katambire, V. N. et al. Forecasting the traffic flow by using ARIMA and LSTM models: case of Muhima junction. *Forecasting* **5**(4), 616–628 (2023).
20. Gao Zichen, Niu Xuejun. 2025 Short-term traffic flow prediction based on STL-GRU-transformer [J/OL]. *Intelligent Computers and Applications*, 1–9 [05–16].
21. Abduljabbar, R. L., Dia, H. & Tsai, P. W. Development and evaluation of bidirectional LSTM freeway traffic forecasting models using simulation data. *Sci. Rep.* **11**(1), 23899 (2021).
22. Geroliminis, N. & Skabardonis, A. Identification and analysis of queue spillovers in city street networks. *IEEE Trans. Intell. Transp. Syst.* **12**(4), 1107–1115 (2011).
23. Wu, X., Liu, H. X. & Gettman, D. Identification of oversaturated intersections using high-resolution traffic signal data. *Transport. Res. Part C Emerg. Technol.* **18**(4), 626–638 (2010).
24. Zhang, L. et al. Control strategy of frequent overflow at intersection based on remote sensing of unmanned aerial vehicle and vehicle trajectory data. *J. Sensors* **2022**(1), 5214240 (2022).
25. Cesme, B. & Furth, P. G. Self-organizing control logic for oversaturated arterials. *Transport. Res. Record J. Transport. Res. Board* **2366**(1), 92–99 (2013).
26. Zhang, L. D., Zhu, W. X. & Ruan, J. H. Coordinated Control Algorithm of Traffic Spillover Intelligent. *Syst. Eng.* **32**(12), 140–144 (2014).
27. Yao, T. et al. Adaptive signal control for overflow prevention at isolated intersections based on fuzzy control. *Transport. Res. Record: J. Transport. Res. Board* **2677**(5), 1387–1401 (2023).
28. Zhao, Y. et al. Various methods for queue length and traffic volume estimation using probe vehicle trajectories. *Transport. Res. Part C: Emerg. Technol.* **107**, 70–91 (2019).
29. Xia Y, Chen J. Traffic flow forecasting method based on gradient boosting decision *Tree[C]//Proceedings of the 2017 5th International Conference on Frontiers of Manufacturing Science and Measuring Technology (FMSMT 2017)*. (Atlantis Press, 2017).
30. Fu, T. et al. Traffic safety oriented multi-intersection flow prediction based on transformer and CNN. *Secur. Commun. Networks* **2023**, 1–13 (2023).
31. Wumaier, H., Gao, J. & Zhou, J. Short-term forecasting method for dynamic traffic flow based on stochastic forest algorithm. *J. Intell. Fuzzy Syst.* **39**(2), 1501–1513 (2020).
32. Ma, C., Dai, G. & Zhou, J. Short-term traffic flow prediction for urban road sections based on time series analysis and LSTM\_BILSTM method. *IEEE Trans. Intell. Transp. Syst.* **23**(6), 5615–5624 (2021).
33. Ounoughi, C. & Yahia, S. B. Sequence to sequence hybrid Bi-LSTM model for traffic speed prediction. *Expert Syst. Appl.* **236**, 121325 (2024).
34. Liu Q (2014) Research on Coordination Control Methods for Oversaturated Traffic Areas Oriented to Overflow Prevention and Evacuation. South China University of Technology.
35. Wang, S. X. et al. Difference research in quota consumption based on regression analysis. *J. Traffic Transport. Eng.* **26**(1), 19–22 (2010).
36. Dejun, K. et al. Local and global sensitivity analysis of LID parameters based on SWMM. *China Water Wastewater* **39**(17), 131–138 (2023).
37. Yue, Z. et al. A multi-spatial scale traffic prediction model based on spatiotemporal transformer. *Comput. Eng. Sci.* **46**(10), 1852–1863 (2024).

## Acknowledgements

This research is supported by the University Natural Sciences Research Project of Anhui Province (grant no. 2023AH040306), the General Project of Anhui Natural Science Foundation (grant no. 2208085ME147), Anhui Province quality project (grant no. 2024xqhz053 and grant no. 2024jyjxggyY261) and Hefei University quality project (grant no. 2024hfujyby01).

## Author contributions

The authors confirm contribution to the paper as follows: Zijun Liang: Conceptualization, Funding acquisition, Project administration, Supervision, Ruihan Wang: Methodology, Writing-Original Draft, Xuejuan Zhan: Resources, Writing-Review & Editing, Tingting Hu: Validation, Xiaoyan Li: Software. Yuqi Li: Writing-Review & Editing.

## Declarations

## Competing interests

The authors declare no competing interests.

### Additional information

**Correspondence** and requests for materials should be addressed to Z.L.

**Reprints and permissions information** is available at [www.nature.com/reprints](http://www.nature.com/reprints).

**Publisher's note** Springer Nature remains neutral with regard to jurisdictional claims in published maps and institutional affiliations.

**Open Access** This article is licensed under a Creative Commons Attribution-NonCommercial-NoDerivatives 4.0 International License, which permits any non-commercial use, sharing, distribution and reproduction in any medium or format, as long as you give appropriate credit to the original author(s) and the source, provide a link to the Creative Commons licence, and indicate if you modified the licensed material. You do not have permission under this licence to share adapted material derived from this article or parts of it. The images or other third party material in this article are included in the article's Creative Commons licence, unless indicated otherwise in a credit line to the material. If material is not included in the article's Creative Commons licence and your intended use is not permitted by statutory regulation or exceeds the permitted use, you will need to obtain permission directly from the copyright holder. To view a copy of this licence, visit <http://creativecommons.org/licenses/by-nc-nd/4.0/>.

© The Author(s) 2025